ALGASED

Remote Sensing for the characterization of
intertidal sediments and microphytobenthic algae
Contribution to WP5 (D5a_2)

Supervised Classification of Hyperspectral Images of ALGASED

Elsy Ibrahim[(1)] and Jaak Monbaliu[(1)]

[(1)]Hydraulics Laboratory,
Department Civil Engineering

Laboratory for Protistology
and Aquatic Ecology

Netherlands Institute for Ecology

The Centre for Environment,
Fisheries and Aquaculture Science

May 2009

http://www.kuleuven.be/hydr/Algased.htm

Supervised Classification of Hyperspectral Images of ALGASED

Table of content

List of Tables

List of Figures

Supervised Classification of Hyperspectral Images of ALGASED

1 Introduction

In the scope of the ALGASED project (*Remote Sensing for the characterization of intertidal sediments and microphytobenthic algae)*, funded by the Belgian Science Policy, hyperspectral imagery was acquired or compiled from previous projects. This imagery is utilized throughout most of the work packages of ALGASED.

This report is a contribution to one of the work packages and falls under the deliverable "Report describing the results on supervised classification on the previously acquired hyperspectral images". In this report, the classification procedure of ALGASED's hyperspectral data is described. This supervised classification is by means of the well known Spectral Angle Mapper (SAM) and the Binary Pairwise Classifier (BPC). SAM determines the spectral similarity between two spectra by calculating the angle between them while BPC discriminates between pairs of classes (Lillesand and Kiefer 2000 and Kumar *et al.* 2000).

2 Methodology

2.1 Available Data

In the archives of ALGASED, there are ten hyperspectral images of the IJzermonding and the Molenplaat. In order to carry out a supervised classification for each image, field data sampled at a timeframe close to that of the image acquisition are required. Therefore, only a few images with accompanying field data could be classified (Table 2.1). These images are briefly described in the coming sections of this report. Yet, for a detailed description of the imagery and details regarding the masking of water of each image, we refer to the report by Ibrahim and Monbaliu (2009a).

Table 2.1: Hyperspectral imagery available accompanied by field data

Area	Sensor	Date of Acquisition	Date of Field Campaign	Image label
IJzermonding	AHS	6/17/2005	6/13/2005	IJ_AHS_05
	CASI	6/12/2007	6/20/2007	IJ_CASI_07
	AHS	6/12/2007	6/20/2007	IJ_AHS_07
Molenplaat	HYMAP	6/8/2004	6/8/2004	MO_HYMAP_04
	AHS	6/23/2005	6/23/2005	MO_AHS_05
	AISA	1/8/2007	6/19/2007	MO_AISA_07

The methods of field sampling and field analysis varied for each campaign. Yet, the major common procedures can be summarized as follows. Field data were sampled at low tide in a time frame close to an overflight (within a couple of months). The coordinates of the sites where the sampling occurred were determined by means of a differential geographical positioning system (DGPS). To account for the variability within a pixel and the uncertainty of hyperspectral image geometric correction, three replicates (or two in some cases) were sampled at each site, with in between distances close to the pixel size, for most field campaigns. Field samples were collected for sample analysis to quantify the following sediment properties: moisture content, mud content, organic matter content, and chlorophyll *a* content (Ibrahim et al. 2009).

2.2 Classes and Field Data

In order to define sediment classes, thresholds are set on sediment properties based on field knowledge and field data analysis. Texture groups are based on mud (grain size diameter <63 μm) volume fractions. Three classes of mud content (MUC), moisture content (MC), chl *a* content, and organic matter content (OM) are defined. These thresholds are based on the physical and biological properties of the sediments and the distribution of the acquired field data (Deronde et al. 2006). These distributions are shown for each field campaign in further sections in the paper, along with the corresponding image. Table 2.2 shows the thresholds for the different classes.

Table 2.2: The sediment classes used for the classification of all the images

Sediment property	Threshold	Class name
Moisture content	0 - 20%	low
	20 - 40%	intermediate
	> 40%	high
Chl *a* content	0 - 40 mg/m^2	low
	40 - 80 mg/m^2	intermediate
	> 80 mg/m^2	high
Mud content	0 - 10%	low
	10 - 40%	intermediate
	> 40%	high
Organic matter content	0 - 4%	low
	4 - 10%	intermediate
	> 10%	high

To label a field sampling location as one of the above mentioned classes of properties, its three replicates are taken into account. When the three replicates all fall in one class of a specific property, the sampling area is considered and labeled as that class. Otherwise, it is disregarded from the study as it indicates too much heterogeneity in the area for a specific property. Therefore, it is not considered to be a reference. For example, when each of the three replicates of a sample has moisture content that falls under the class of low MC, the sample is considered to contain low MC; else, it is disregarded from the analysis. In case there were no replicates in a field campaign, and only one sample was taken for a sampling location, a field sample would be then labeled according to this one sample. Appendix 1 shows the useful sampling locations that were used as references for the classification of the different images.

After labeling the samples and disregarding the non-homogeneous areas, GPS coordinates of each reference sampling location are used to locate it on the corresponding hyperspectral image. In order to include the replicates and keep in mind geometrical inaccuracies of an image and the GPS measurements, a 3×3 pixel quadrant is considered to represent a sampling site on the image, where the central pixel is the pixel indicated by the GPS measurement.

2.3 Spectral Angle Mapper

2.3.1 Overview

The Spectral Angle Mapper (SAM) is a physically-based classification using an n-dimensional angle to match pixels to certain reference spectra. Each spectrum in an image is treated

as a vector with a dimensionality equal to the number of bands in the image. SAM determines spectral similarity by calculating the angles between spectra. The smaller the angle is, the larger the similarity between the pixels. Moreover, pixels further from a specified maximum angle threshold in radians are not classified.

To calculate the spectral angle, consider pixels reflectance values in an image and reflectance of some reference spectra. If a vector is drawn from the origin through each point, the angle between any two vectors constitutes the spectral angle between those two points. Figure 2.1 shows a 2-dimentional example. SAM computes a spectral angle between each pixel spectrum and each reference spectrum. The smaller the spectral angle is, the more similar the pixel and reference spectra. Yet, SAM is insensitive to illumination as it uses only vector direction and not vector length. Therefore, a darker pixel would be plotted along the same vector, but closer to the origin (Kruse et al. 1993, Lillesand and Kiefer 2000).

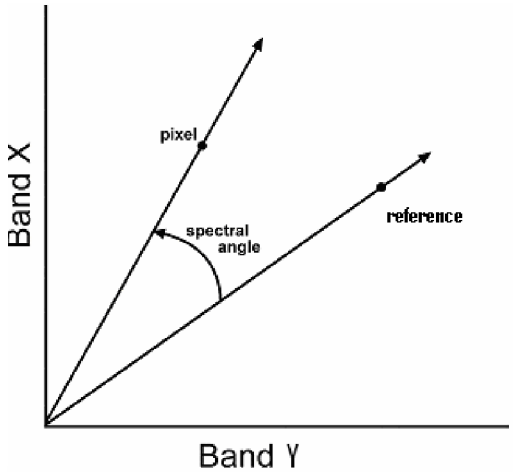

Figure 2.1: Sediment property distributions based on 2005 field measurements on the IJzermonding

The classification of the images in this report is carried out for individual sediment properties where the results of the classification are distribution maps of each sampled sediment property. Therefore, each sediment property is taken separately. By comparing the spectra in an image to some chosen reference spectra of a specific sediment class, classification is possible. The field data is utilized to recognize the reference spectra in an image. The rest of the spectra in the image would refer to those reference spectra for classification. Therefore, when classifying an image, all the chosen reference spectra for a class are averaged and used leading to an overall representative spectrum of the reference data. Then, the reflectance spectrum of each pixel is compared to this reference spectrum. When an angle is smaller than a specified threshold angle, the pixel is assigned to that class. If the angle exceeded the threshold, the pixel is not classified. For these Sam calculations, the SAM code in ENVI 4.6 was used.

SAM does not include any feature selection from the hyperspectral data. Yet, it normalizes the spectra by not dealing with vector length in the calculations. This leads to an emphasis on different shapes of spectra, i.e. on absorption features. Therefore, the classification for this report is carried out using all the bands of each image. Yet, since many bands are contiguous and contain redundant information, an experiment to select five bands from each image is also carried out in this report. Based on the ALGASED report by Ibrahim and Monbaliu (2008) four, five, or six bands chosen from the hyperspectral images can be a simple and sufficient selection to retrieve similar or better information than using all the bands. To test this for SAM classification, five bands are selected: 1) a band in the blue (B) part of the spectrum, 2) band in the green (G) part of the

spectrum, 3) the band resulting in the lowest reflectance at the chl *a* dip, 4) a band in the near infra-red part of the spectrum (NIR), and 5) a shortwave infra-red (SWIR) band.

2.3.2 Accuracy Assessment

The choice of the SAM threshold angle is one of the indications of the similarity between pixels. The higher the threshold angle, the less spectrally similar the pixels are. In this report, a common and low threshold value of 0.10 radians was used to retrieve the most similar pixels.

In order to quantify the accuracy of the classification, the field data were also used by calculating the percentage of correct classification of the sampling sites, both as 3×3 pixel groups and as central pixels. In case a reference sampling site was not classified, it was considered as wrongly classified.

2.4 Bayesian Pairwise Classifier

2.4.1 Overview

If given an image to be classified into "c" number of classes, the Baysian Pairwise Classifier (BPC) decomposes it into a set of simpler $\binom{c}{2}$ two-class problems where each has its own feature space and classifier that are independently trained. Furthermore, the Bayesian classifiers model the probability density functions (pdf) of the classes studied in each pair into a feature space. The estimation of these pdfs conditioned on a single feature, i.e. band, also affects the feature selection. In order to model these pdfs, a mixture of Gaussians approach is used (Kumar *et al.* 2000) A forward feature selection algorithm is then used to grow the feature space, and an efficient technique is developed to obtain a mixture of Gaussians in the larger feature space from the mixture of Gaussians in the smaller spaces (Kumar et al. 2000). This methodology then results in classification accuracy and the identification of the most important features in separating a pair of classes. The BPC code by the remote sensing lab at Purdue University (Kumar et al. 2000) was used for this report.

To carry out the classification, the reference samples from the field data were also considered. Contrary to SAM, these samples were divided into two groups: training samples and validation samples. The training samples were used to carry out the classification and the feature selection, while the validation set tested the accuracy of the classification.

In general, it is preferred to have 50 % of the samples in each group. The field data available is limited compared to the number of bands of hyperspectral imagery. As a rule of thumb, it is normally considered to have a reliable classification and feature selection when the number of training data exceeds the number of features at least by one. Since most of the time this is not attainable for hyperspectral images, this report experiments the usage of the BPC code with the limited amount of data. Therefore, due to statistical requirements for the models, it was occasionally required that more than 50 % of the reference data would be used for training, and less for validation.

2.4.2 Accuracy Assessment

As the results of BPC are based on a pair-wise system, a voting method was used to determine a pixel's label. Therefore, each pixel was referred to the class label selected by the most $\binom{c}{2}$ classifiers.

3 Results: IJzermonding

3.1 2005 - AHS

This image was taken on the 17th June, 2005 and has a 3.42 m × 3.42 m pixel size. It contains 19 useful bands covering the visible (VIS), near infra-red (NIR) and shortwave infra-red (SWIR) parts of the spectrum. Prior to classification, water areas were masked out of the image. Vegetation was masked out by putting a threshold of 0.30 on the normalized difference vegetation index (NDVI) calculated by the central bands of the red and NIR parts of the spectrum. The properties sampled in the corresponding field campaign are MC, MUC, chl *a* content, and OM content. Figure 3.1 shows the distribution of these properties in the field data. The total number of observations for MC is 82, for mud content is 86, for chl *a* content is 84, and for OM content is 81.

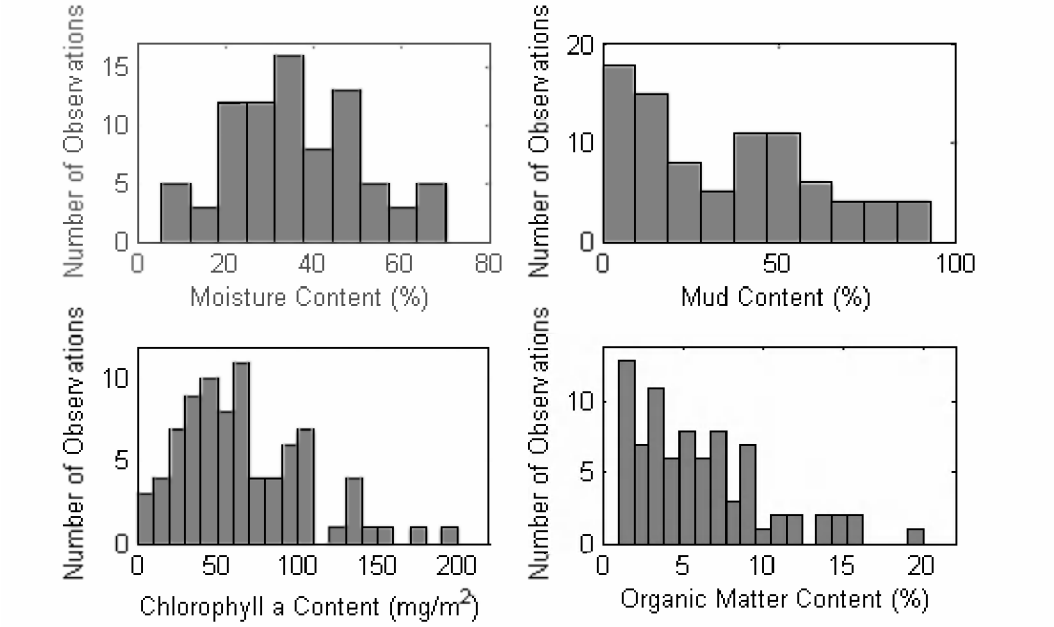

Figure 3.1: Sediment property distributions based on 2005 field measurements on the IJzermonding

The image is classified by BPC using feature selection and SAM using all bands. Furthermore, it was also classified by SAM with five bands only shown in Table 3.1 with their central wavelength and the full width at half maximum (FWHM).

Table 3.1: The five selected bands from IJ_AHS_05

Band	Wavelength (µm)	FWHM (µm)
2	0.484	0.028
4	0.542	0.028
9	0.689	0.028
14	0.833	0.028
21	1.622	0.159

3.1.1 Chl *a*

i. Reference and training data

To categorize chl *a*, three classes were identified, low chl *a* (4 sampling sites), intermediate chl *a* (5 sampling sites), and high chl *a* (2 sampling sites). Each sampling site was referred to by 3 × 3 pixels, leading to 99 reference pixels. Figure 3.2 shows the mean spectra corresponding to the reference pixels of each class.

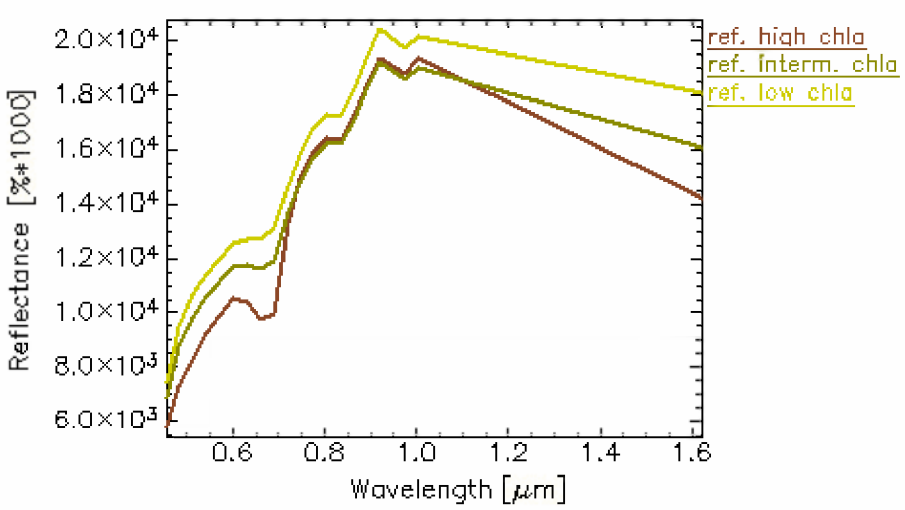

Figure 3.2: Mean spectra of reference pixels for each chl *a* class (IJ_AHS_05)

ii. SAM

To classify the whole image, angles of 0.2 and 0.3 radians were required when using all the bands or the five chosen bands (Table 3.1) respectively. Figure 3.3 shows the resulting classified images and means of reflectance spectra per class, with an angle of 0.10 radians. Figure 3.4 shows the classification result of using only five bands with a threshold angle of a 0.20 radians. Table 3.2 shows the classification accuracies obtained for the results.

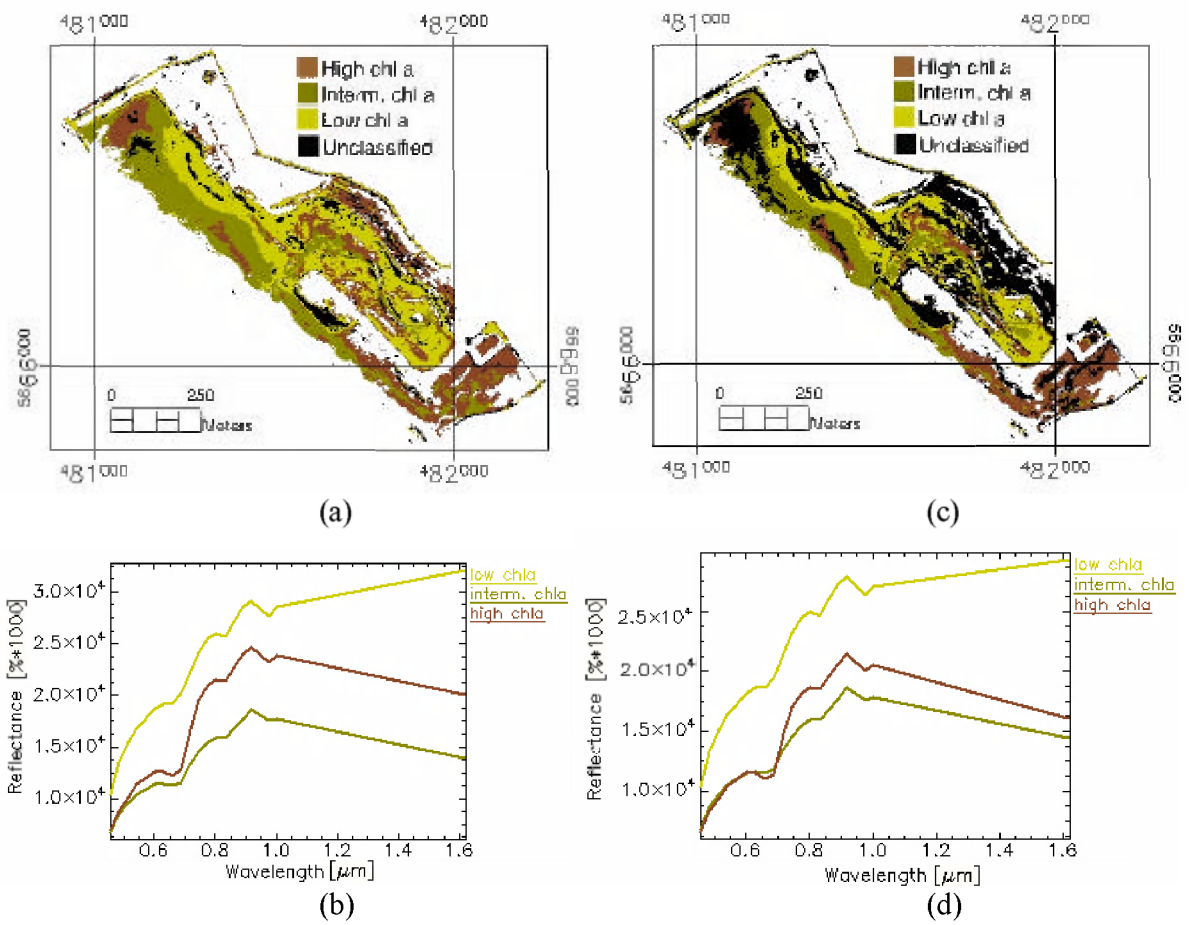

Figure 3.3: Classification results and mean spectra for IJ_AHS_05 - chl *a* with a threshold angle of 0.10 radians (a) and (b) all bands; (c) and (d) five bands

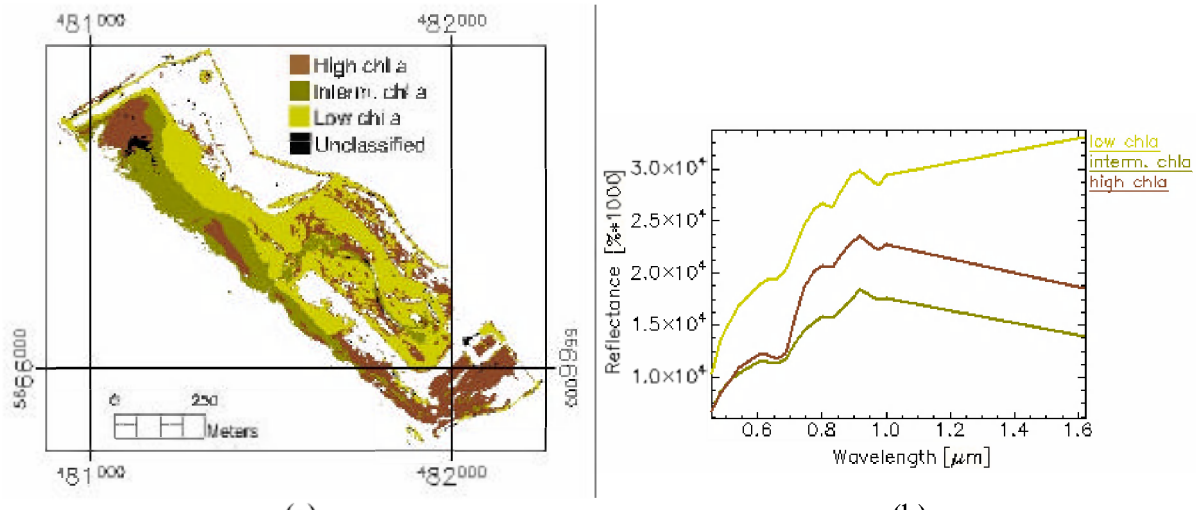

Figure 3.4: Classification results and mean spectra for IJ_AHS_05 - chl *a* with a threshold angle of 0.20 radians and five band selection

Table 3.2: Classification accuracy results IJ_AHS_05– chl *a*

threshold angle (radians)	Features	classification accuracy (%) and the number of unclassified locations			
		3x3 pixels	unclassified locations	central pixel	unclassified locations
0.1	all bands	46	0	73	0
0.1	five bands	46	0	55	0
0.2	five bands	55	0	64	0

iii. BPC

To classify chl *a*, 50% of the available data were used for training and the remaining 50% were used for validation. The classification was carried out ten times where for each run, a random choice of training and validation pixels was done. The average validation accuracy of the ten runs was 74 % with a standard deviation of 11 %. The run with the highest accuracy of 89.18 % resulted in the classified image shown in Figure 3.5. Table 3.3 shows the features selected to discriminate a pair of classes.

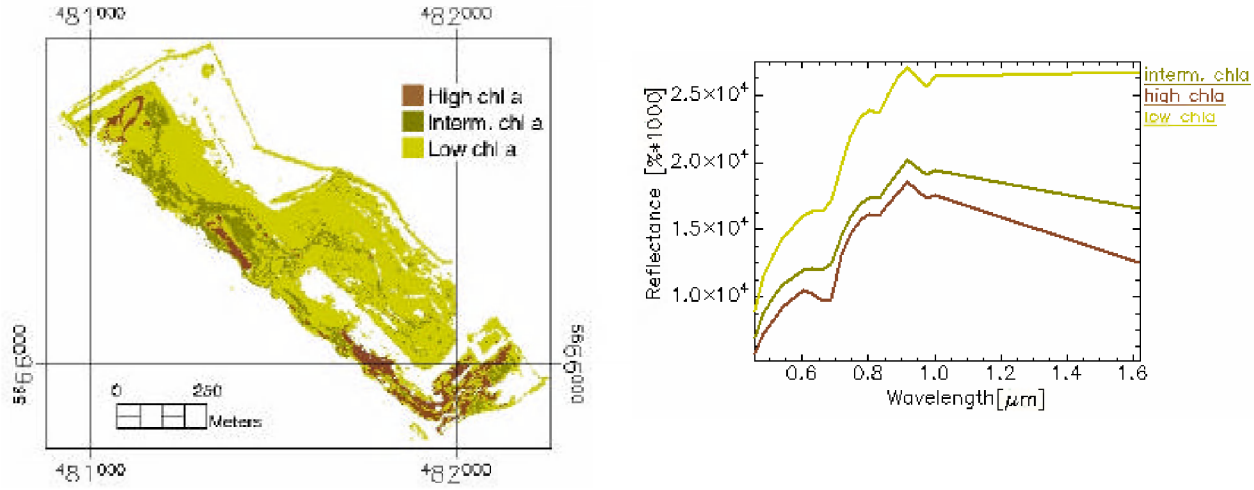

(a) (b)

Figure 3.5: Classification results and mean spectra for IJ_AHS_05 – chl *a*

Table 3.3: The results of feature selection for each pair of classes (IJ_AHS_05 - chl *a*)

Class (1)	Class (2)	Number of features selected	Features (nm)
Low chl *a*	Interm. chl *a*	3	1(455), 10(718), 17(918)
Low chl *a*	High chl *a*	3	9(689), 10(718), 18(948)
Interm. chl *a*	High chl *a*	1	1(455)

3.1.2 Moisture Content

i. Reference and training data

To categorize moisture content, three classes were identified, low MC (3 sampling sites), intermediate MC (11 sampling sites), and high MC (7 sampling sites). Each sampling site was referred to by 3 × 3 pixels, leading to 189 reference pixels. Figure 3.6 the mean spectra corresponding to the reference pixels of each class.

.

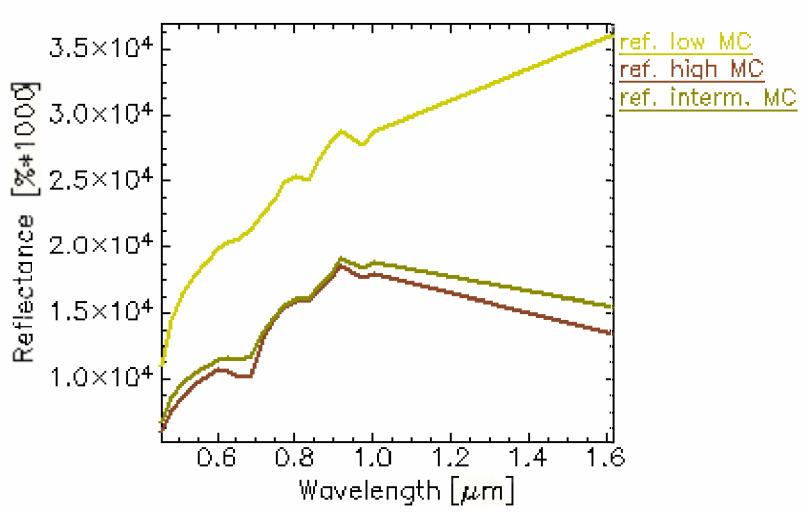

Figure 3.6: Mean spectra of reference pixels for each MC class (IJ_AHS_05)

ii. SAM

To classify the whole image, angles of 0.20 and 0.30 radians were required while using all the bands or the five chosen bands (Table 3.1) Figure 3.7 and Figure 3.8 show the results of the classification for 0.10 and 0.20 radians. Table 3.4 shows the classification accuracies obtained.

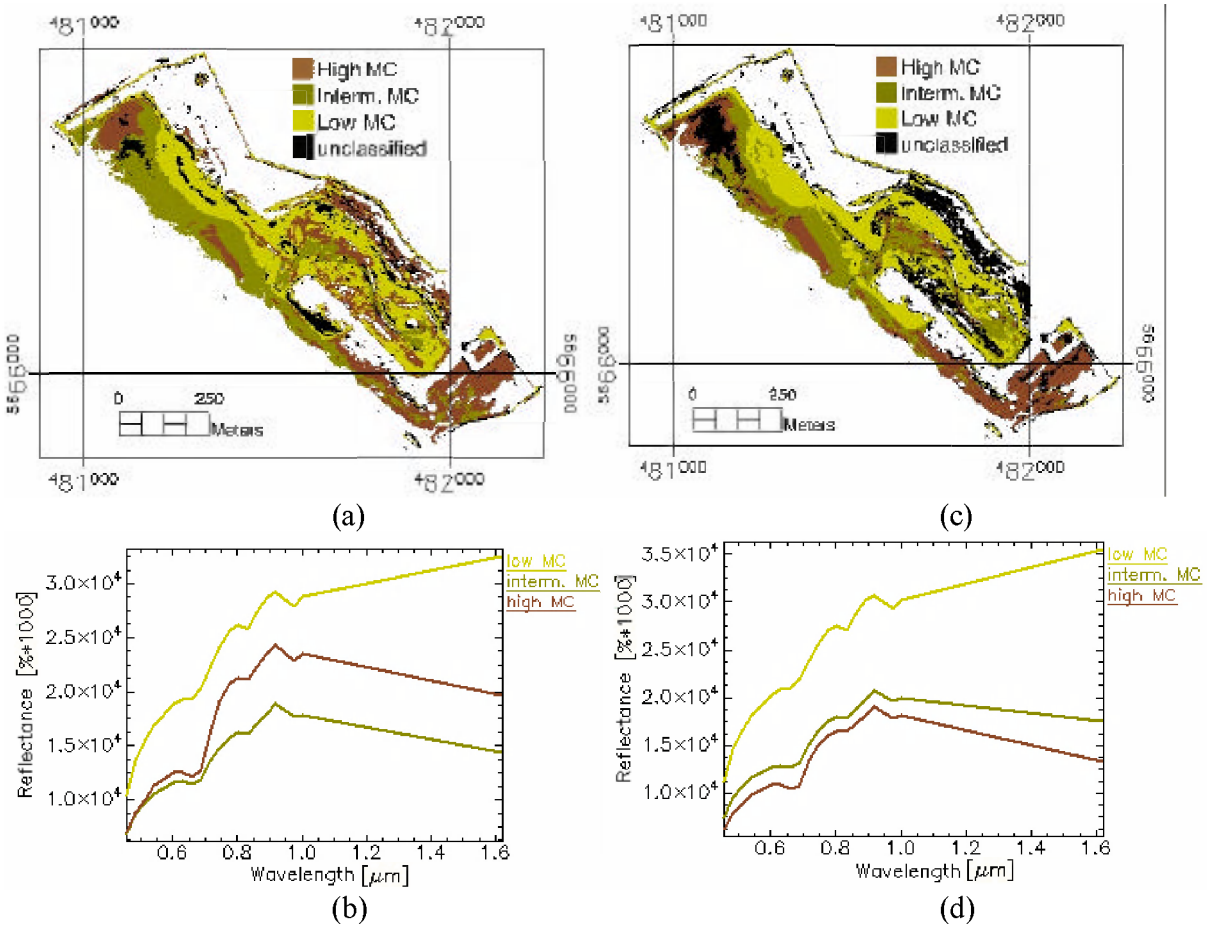

Figure 3.7: Classification results and mean spectra for IJ_AHS_05-MC with a threshold angle of 0.10 radians (a) and (b) all bands; (c) and (d) five bands

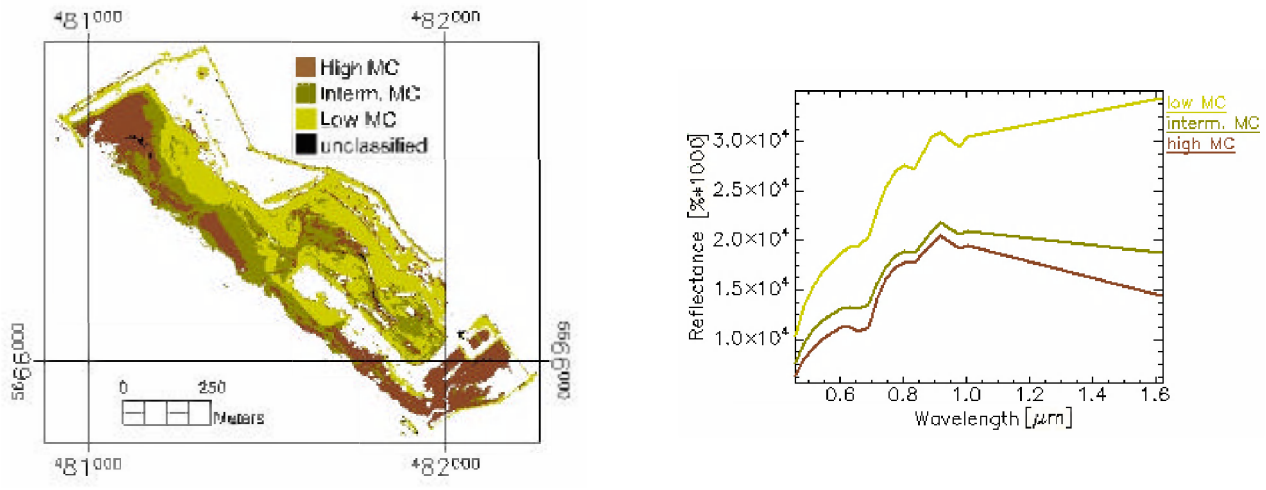

(a) (b)

Figure 3.8: Classification results and mean spectra for IJ_AHS_05 MC with a threshold angle of 0.20 radians and five band selection

Table 3.4: Classification accuracy results IJ_AHS_05 – MC

threshold angle (radians)	Features	classification accuracy (%) and the number of unclassified locations			
		3x3 pixels	unclassified locations	central pixel	unclassified locations
0.1	all bands	48	3	76	1
0.1	five bands	48	0	57	0
0.2	five bands	48	0	81	0

iii. BPC

To classify moisture content, 60% of the available data were used for training and the remaining data were used for validation. The classification was carried out ten times where for each run, a random choice of training and validation pixels was done. The average classification accuracy of 10 runs of the pixels used for validation was 95 % with a standard deviation of 4 %. The run with the highest accuracy of 100 % resulted in the classified image shown in Figure 3.9. Table 3.5 shows the features selected to discriminate a pair of classes.

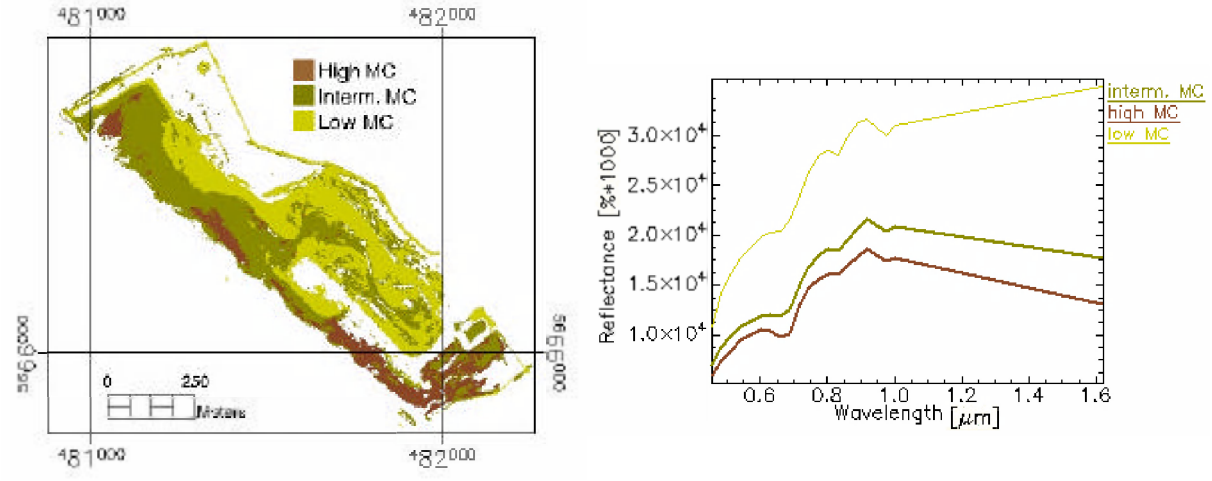

(a) (b)

Figure 3.9: Classification results and mean spectra for IJ_AHS_05 – MC

Table 3.5: The results of feature selection for each pair of classes (IJ_AHS_05 – MC)

Class (1)	Class (2)	Number of features selected	Features (nm)
Low MC	Interm. MC	1	3(513)
Low MC	High MC	2	21(1622),12(774)
Interm. MC	High MC	5	9(689),21(1622),3(513),4(542),19(975)

3.1.3 Mud content

i. Reference and training data

To categorize mud content, three classes were identified, low MUC (5 sampling sites), intermediate MUC (6 sampling sites), and high MUC (9 sampling sites). Each sampling site was referred to by 3 × 3 pixels, leading to 180 reference pixels. Figure 3.10 the mean spectra corresponding to the reference pixels of each class..

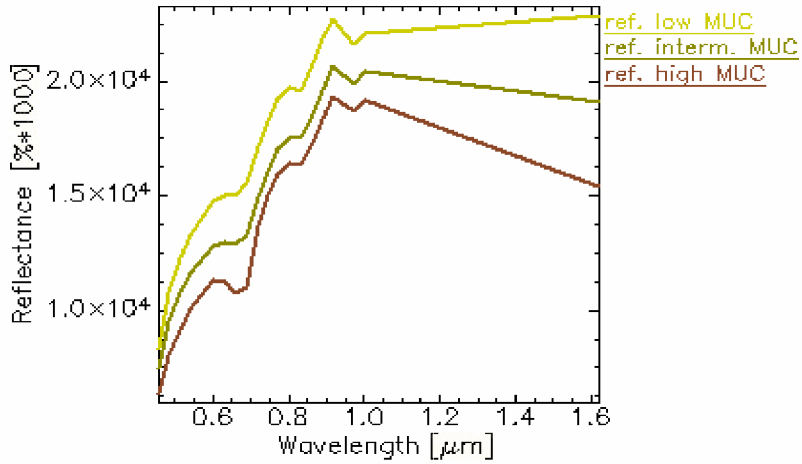

Figure 3.10: Mean spectra of reference pixels for each MUC class (IJ_AHS_05)

ii. SAM

To classify the whole image, angles of 0.2 and 0.3 radians were required while using all the bands or the five chosen bands (Table 3.1) respectively. Figure 3.11 and Figure 3.12 show the resulting classified images and mean reflectance spectra of the resulting classes with an angle of 0.10 and 0.20 radians. Table 3.6 shows the classification accuracies obtained for the results.

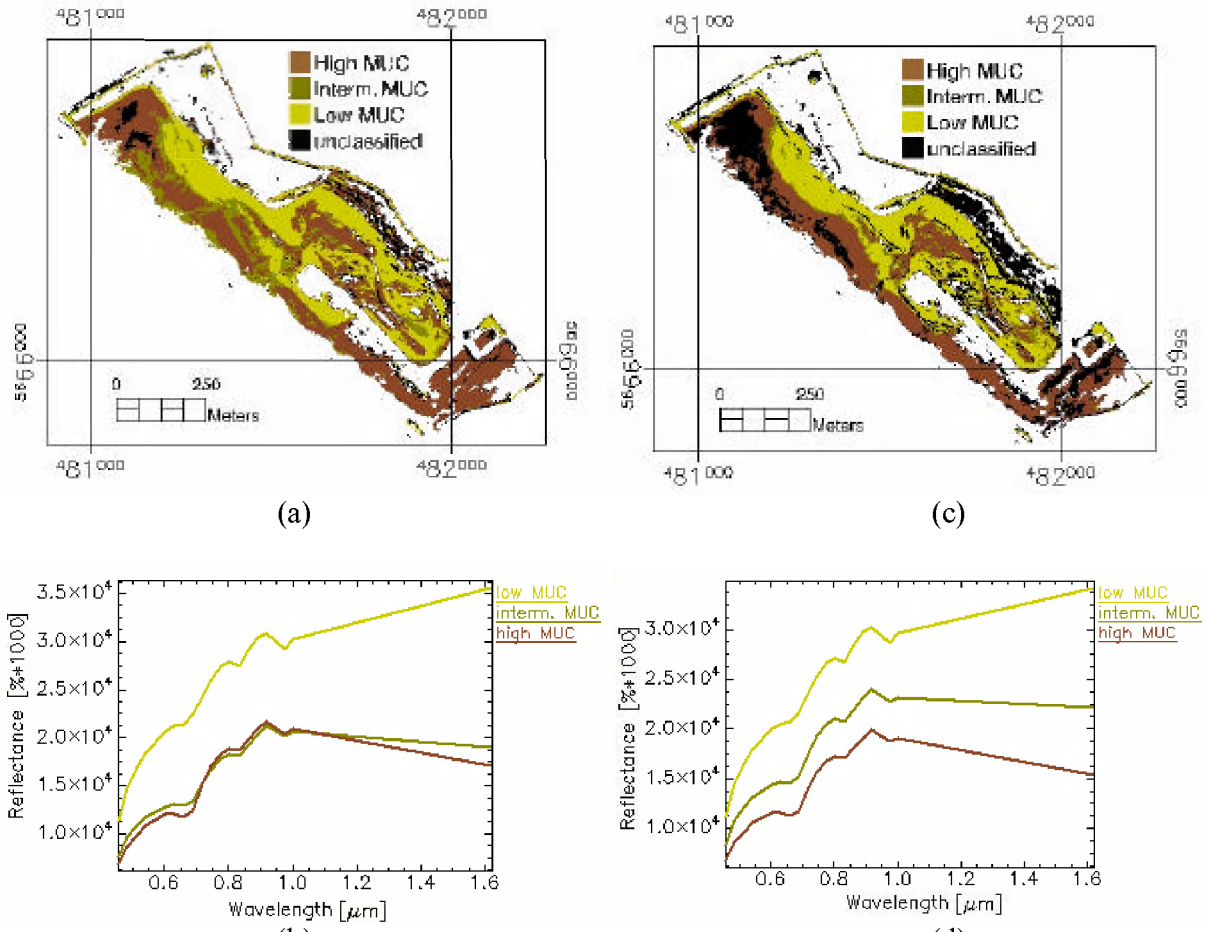

Figure 3.11: Classification results and mean spectra for IJ_AHS_05-MUC with a threshold angle of 0.10 radians (a) and (b) all bands; (c) and (d) five bands

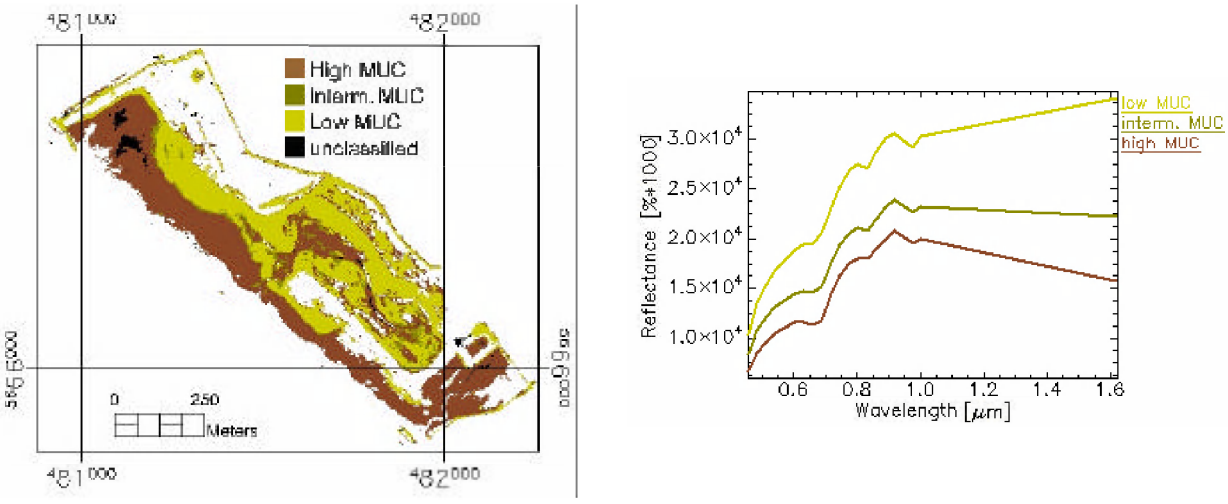

Figure 3.12: Classification results and mean spectra for IJ_AHS_05 MUC with a threshold angle of 0.20 radians and five band selection

Table 3.6: Classification accuracy results IJ_AHS_05 – MUC

threshold angle (radians)	Features	classification accuracy (%) and the number of unclassified locations			
		3x3 pixels	unclassified locations	central pixel	unclassified locations
0.1	all bands	45	0	55	0
0.1	five bands	40	3	50	1
0.2	five bands	45	0	50	0

iii. BPC

To classify mud content, 65% of the available data were used for training and the remaining data were used for validation. The classification was carried out only four times, where for each run, a random choice of training and validation pixels was done. The average validation accuracy of the ten runs was 74 % with a standard deviation of 7 %. The run with the highest accuracy resulted in 83 % (Figure 3.13). Table 3.7 shows the features selected to discriminate a pair of classes.

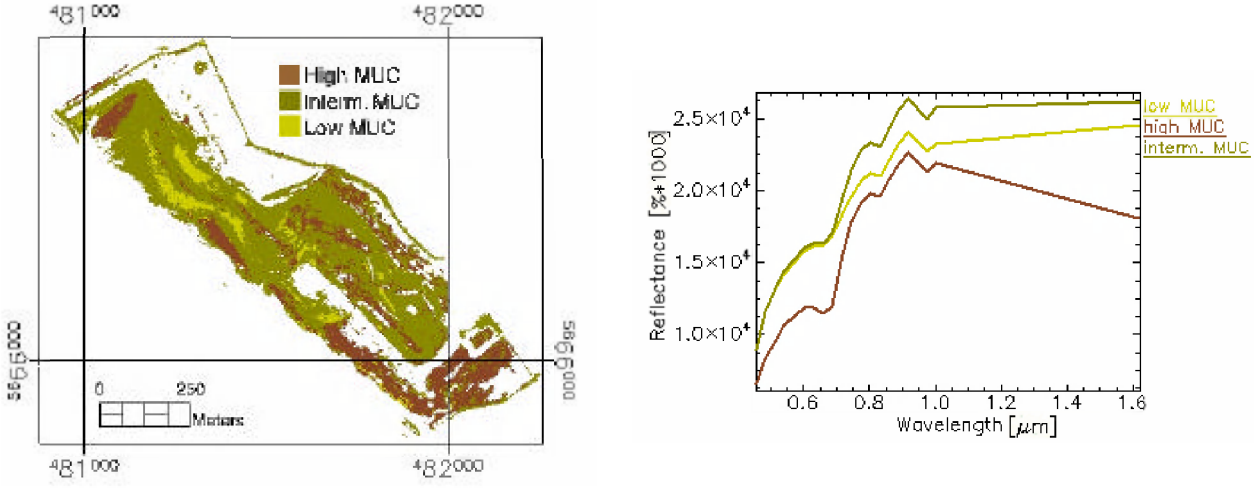

(a) (b)

Figure 3.13: Classification results and mean spectra for IJ_AHS_05 – MUC

Table 3.7: The results of feature selection for each pair of classes (IJ_AHS_05 – mud content)

Class (1)	Class (2)	Number of features selected	Features(nm)
Low MUC	Interm. MUC	6	18(1004),19(1622),11(774),1(455),4(542),6(630)
Low MUC	High MUC	4	18(1004),8(689),4(542),14(682)
Interm. MUC	High MUC	5	2(484),4(542),7(659),18(1004),8(689)

3.1.4 Organic matter

i. Reference and training data

To categorize mud content, three classes were identified, low OM (7 sampling sites), intermediate OM (8 sampling sites), and high OM content (2 sampling sites). Each sampling site was referred to by 3 × 3 pixels, leading to 153 reference pixels. Figure 3.14 the mean spectra corresponding to the reference pixels of each class.

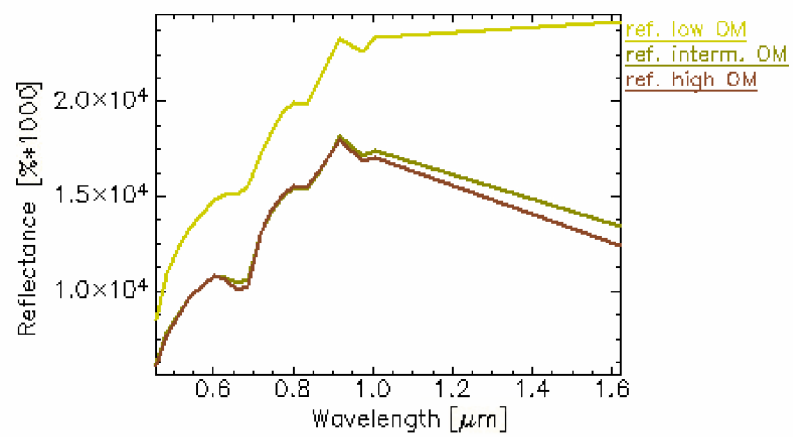

Figure 3.14: Mean spectra of reference pixels for each OM class (IJ_AHS_05)

ii. SAM

To classify the whole image, angles of 0.2 and 0.3 radians were required while using all the bands or five bands (Table 3.1) respectively. Figure 3.15 and Figure 3.16 show the resulting classified images and mean reflectance spectra of the resulting classes with an angle of 0.10 and 0.20 radians. Table 3.8 shows the classification accuracies obtained for the results.

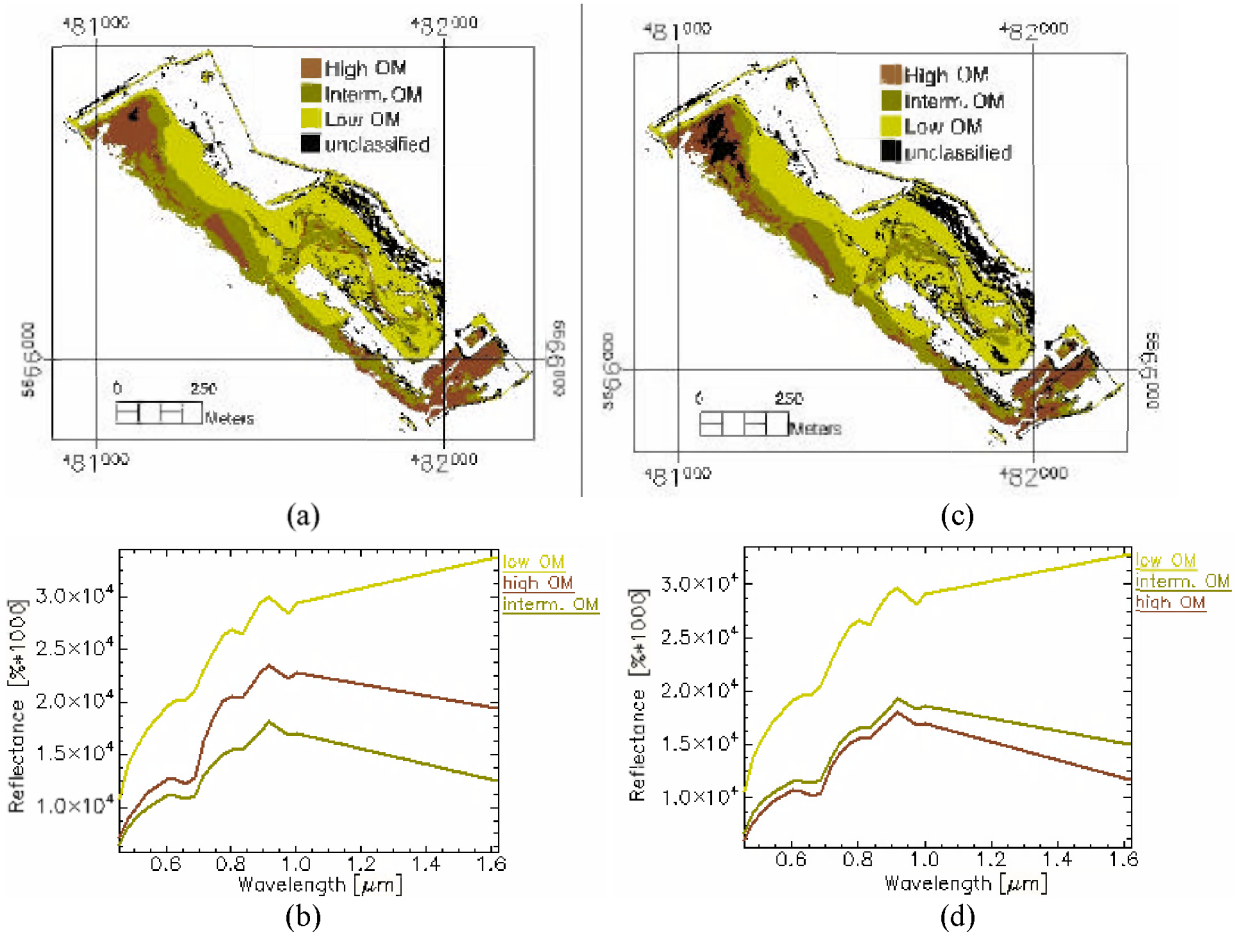

Figure 3.15: Classification results and mean spectra for IJ_AHS_05 - OM with a threshold angle of 0.10 radians (a) and (b) all bands; (c) and (d) five bands

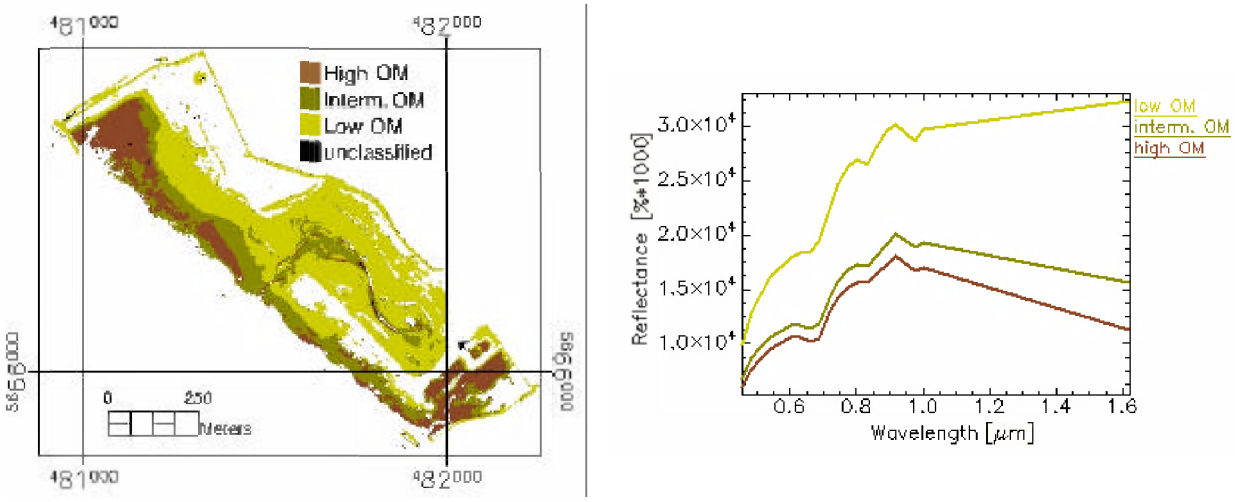

(a) (b)

Figure 3.16: Classification results and mean spectra for IJ_AHS_05 OM with a threshold angle of 0.20 radians and five band selection

Table 3.8: Classification accuracy results IJ_AHS_05 – OM

threshold angle (radians)	Features	classification accuracy (%) and the number of unclassified locations			
		3x3 pixels	unclassified locations	central pixel	unclassified locations
0.1	all bands	24	0	65	0
0.1	five bands	29	0	53	0
0.2	five bands	29	0	53	0

iii. BPC

To classify organic matter, 50% of the available data were used for training and the remaining data were used for validation. The classification was carried out ten times where for each run, a random choice of training and validation pixels was done. The average validation accuracy of the ten runs was 66 % with a standard deviation of 12 %. The run with the highest accuracy was of 99 % (Figure 3.17). Table 3.9 shows the features selected to discriminate the pairs of classes.

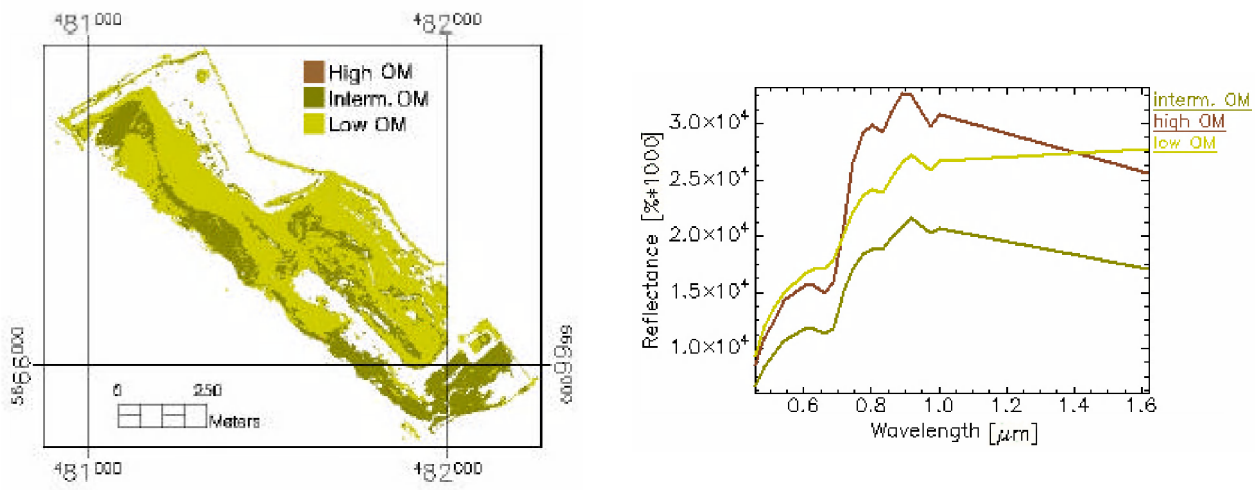

Figure 3.17: Classification results obtained for IJ_AHS_05 – OM

Table 3.9: The results of feature selection for each pair of classes (IJ_AHS_05 – organic matter content)

Class (1)	Class (2)	Number of features selected	Features
Low OM	Interm. OM	5	5(601),8(689),17(975),2(484),9(718)
Low OM	High OM	4	17(1004),15(891),12(804),6(630)
Interm. OM	High OM	5	17(975),14(862),15(891),19(1622),12(804)

3.1.5 Discussion and conclusions

Observing the results of the different properties in general, the correlation between the four properties was noticed. For example, the areas where high chl *a* is present, the mud content, moisture content, and organic matter content were also relatively high.

There were three aspects to compare in the above results: SAM with all the spectral bands of the image, SAM with five bands of the image (Table 3.1), and BPC with feature selection. The use of low thresholds of 0.10 rad and 0.20 rad indicates a high spectral similarity between the classified pixels. Yet, when referring to the field data for the classification accuracy, it is generally low. It must be noted that the number of field data was too low to reach a comprehensive conclusion. The classification accuracies of BPC were relatively high. Yet, similarly to SAM, the number of field data used was too low to result in a comprehensive overview of the classification accuracy.

When comparing the mean reference spectra to the mean spectra resulting from the classification, the following conclusions can be seen. First, regarding chl *a* content, the spectra of the SAM classification with five bands (Figure 3.3(d) and Figure 3.4(b)) do not resemble the reference spectra (Figure 3.2). Yet, the mean spectra of the BPC classification results (Figure 3.5(b)) resemble the reference spectra (Figure 3.2). Second, for moisture content, the spectra of the SAM classification with five bands (Figure 3.7(d) and Figure 3.8(b)) and the BPC classification resemble the reference spectra (Figure 3.6). Yet, the mean spectra of the SAM classification using all the bands (Figure 3.7 (b)) are quite different from the reference spectra (Figure 3.6) (especially with high and interm. classes). Third, regarding mud content, the mean reference spectra (Figure 3.10) are similar to the spectra of the results of SAM classification with five bands (Figure 3.11(d) and Figure 3.12(b)), yet, dissimilar to the mean spectra of the BPC classes (Figure 3.13(b)) and SAM classification using all the bands (Figure 3.11(b)). Finally, the mean spectra of the different

results of organic matter content are quite different from each other (Figure 3.14, Figure 3.15, Figure 3.16, Figure 3.17).

A comparison was also drawn between SAM classifications using all the bands versus using only five bands. It was seen that when five bands were used, a higher threshold angle was required to classify an area similar to that classified when all the bands were used. Yet, an angle of 0.2 radians still refers to a high similarity between the data classified in one class. Comparing the results obtained by all the bands using a threshold angle of 0.10 radians to using five bands and an angle of 0.20 radians, the results were quite similar in most cases if we refer to the classification accuracy. Yet, they are different when it to the resulting classes and their mean reflectance values.

Furthermore, a comparison was also drawn between the results of SAM and BPC. For chl *a* content, the results of the BPC show more dominance of low chl *a* areas (Figure 3.5). Regarding moisture content, the results of the BPC were quite similar to those SAM (Figure 3.7, Figure 3.8, and Figure 3.9). On the other hand, mud content was classified quite differently by means of SAM with all the bands, SAM with five bands, and BPC (Figure 3.11, Figure 3.12, and Figure 3.13). Finally, for the organic matter content classification, the high OM matter content almost disappeared in the results of BPC (Figure 3.17).

The feature selection carried out while applying the BPC resulted in specific bands used to classify the different properties (Table 3.3, Table 3.5, Table 3.7, and Table 3.9). The SWIR band was only used to differentiate the different classes of MC (Table 3.5). This corresponded to the fact that the reflectance of SWIR is quite sensitive to moisture content.

In the results above, only the SAM classification results with the thresholds of 0.10 radians and 0.20 radians are shown. The results of higher thresholds are in the report Ibrahim and Monbaliu (2009b)

3.2 2007 – AHS

This image was taken on the 12th June, 2007 at low tidal conditions. The image has a 3 m × 3 m pixel size and has various unusable bands in the SWIR region. It contains 38 non-corrupt channels covering the VNIR and SWIR parts of the spectrum. Prior to classification, water and vegetation were masked out of the image. The properties sampled in the corresponding field campaign are MC, MUC, and chl *a* content. Figure 3.18 shows the distributions of these properties in the field data. The total number of observations for MC is 48, for mud content is 54, and for chl *a* content is 56.

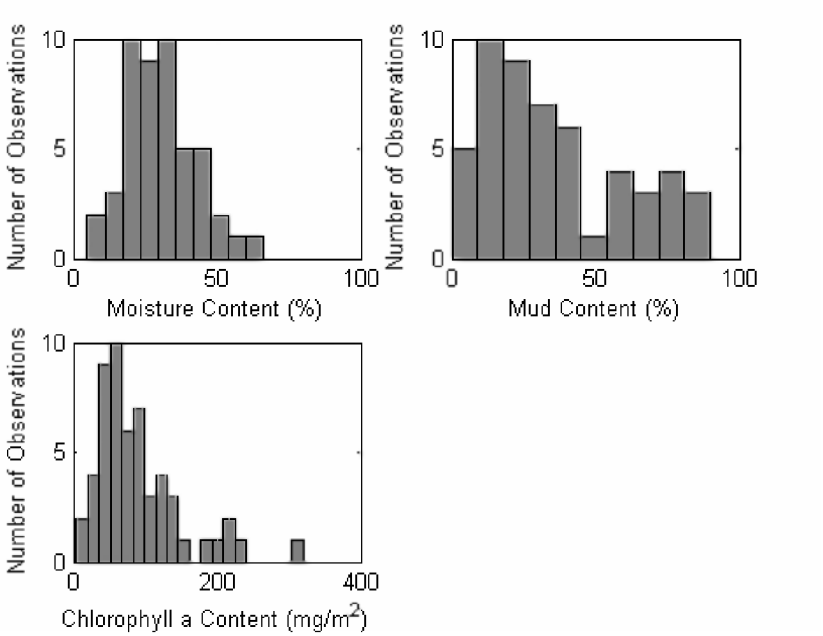

Figure 3.18: Sediment property distributions based on 2007 field measurements on the IJzermonding

The image was classified using SAM using all the available bands and only the five bands shown in Table 3.10. The image was not classified by BPC due to technical difficulties with the codes. More work is being done regarding the issue.

Table 3.10: The five selected bands from IJ_AHS_07

band	Wavelength (nm)	FWHM (nm)
2	482	29.5
4	539	32.2
8	653	32.1
14	825	32.1
21	1585.8	91.0

3.2.1 Chla

i. Reference and training data

To categorize chl *a*, three classes were identified, low (6 sampling sites), intermediate (15 sa mpling sites), and high (21 sampling sites). Although each sampling site in this field campaign was sampled once, each sampling site was referred to in the image by 3 × 3 pixels, leading to 378 reference pixels. Figure 3.19 the mean spectra corresponding to the reference pixels of each class.

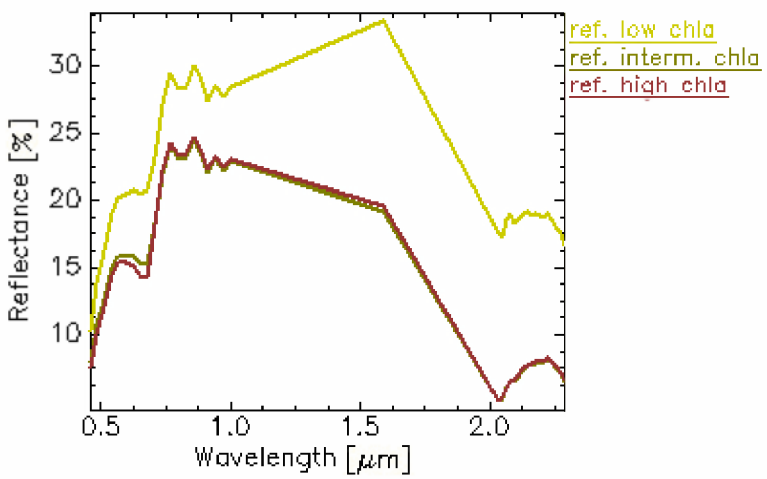

Figure 3.19: Mean spectra of reference pixels for each class (IJ_AHS_07)

ii. SAM

To classify the whole image, an angle of 0.30 radians was required while using all the bands or five bands (Table 3.10). Figure 3.20 and Table 3.11 show the results of the classification.

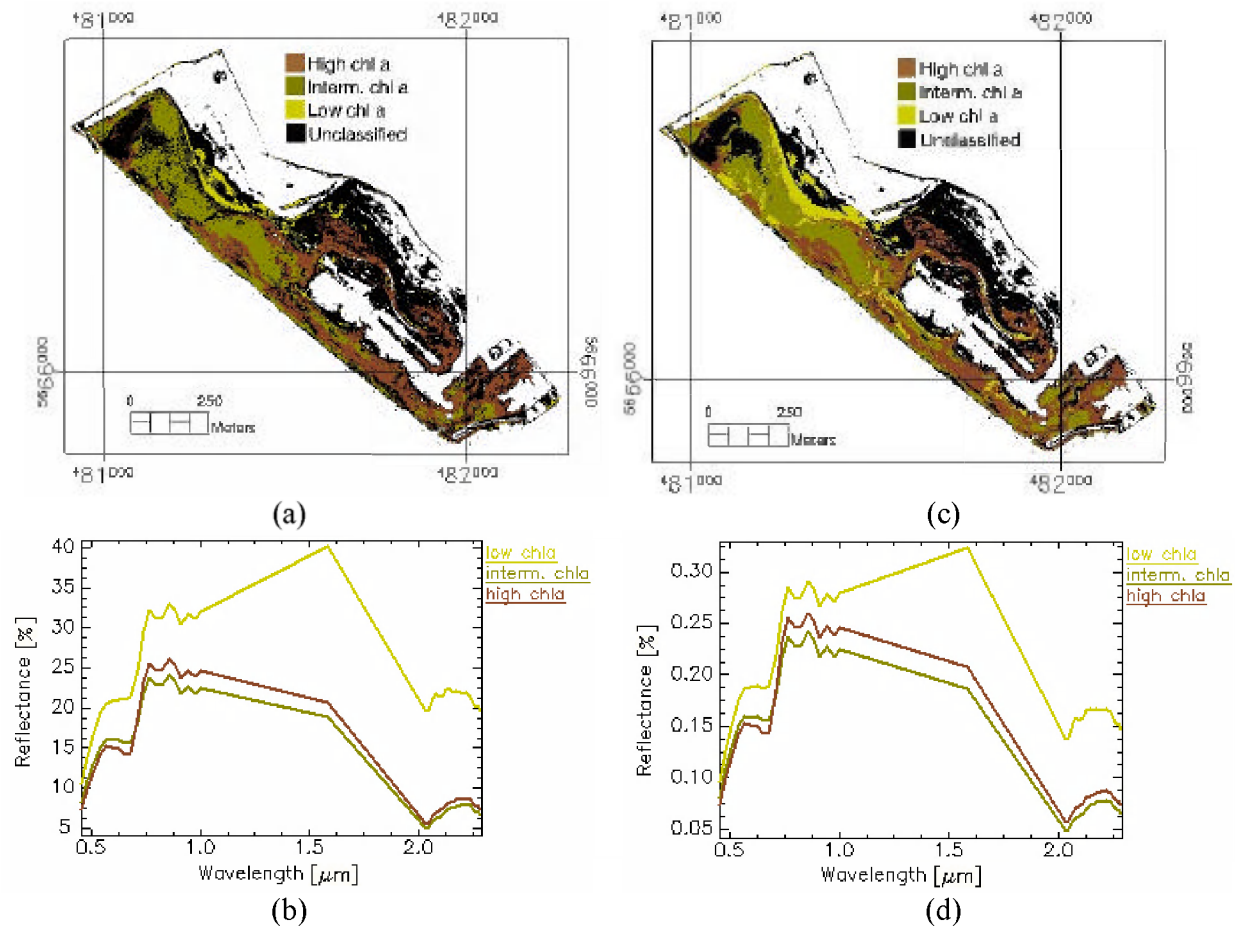

Figure 3.20: Classification results and mean spectra for IJ_AHS_07 – chl *a* with a threshold angle of 0.10 radians (a) and (b) all bands; (c) and (d) five bands

Table 3.11: Classification accuracy results IJ_AHS_07 – chl *a*

threshold angle (radians)	Features	classification accuracy (%) and the number of unclassified locations			
		3x3 pixels	unclassified locations	central pixel	unclassified locations
0.1	all bands	10	21	49	7
0.1	five bands	24	3	49	5

iii. BPC

Due to format incompatibility between the BPC code and the AHS image, it is not possible to have a classification for chl *a*.

3.2.2 Moisture Content

i. Reference and training data

To categorize MC, three classes were identified, low MC (5 sampling sites), intermediate MC (12 sampling sites), and high MC (6 sampling sites). Each sampling site was referred to by 3×3 pixels, leading to 345 reference pixels. Figure 3.21 the mean spectra corresponding to the reference pixels of each class.

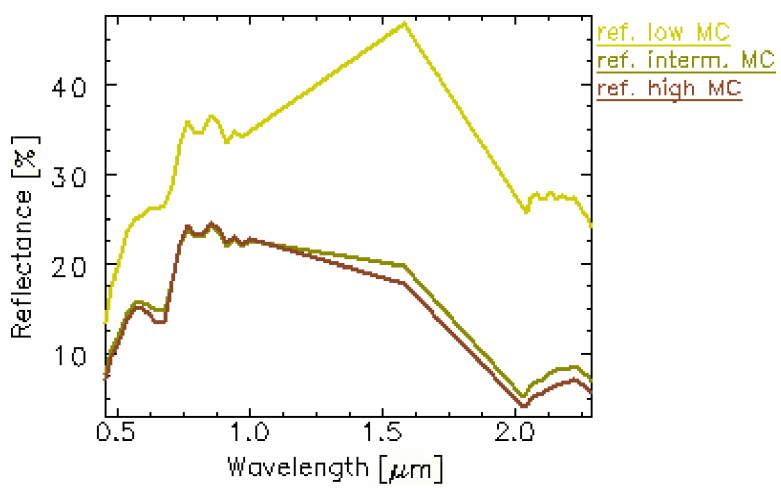

Figure 3.21: Mean spectra of reference pixels for each class (IJ_AHS_07)

ii. SAM

To classify the whole image, an angle of 0.30 radians was required while using all the bands or five bands (Table 3.10). Figure 3.22 shows the results of the classification. Table 3.12 shows the classification accuracies obtained for the results.

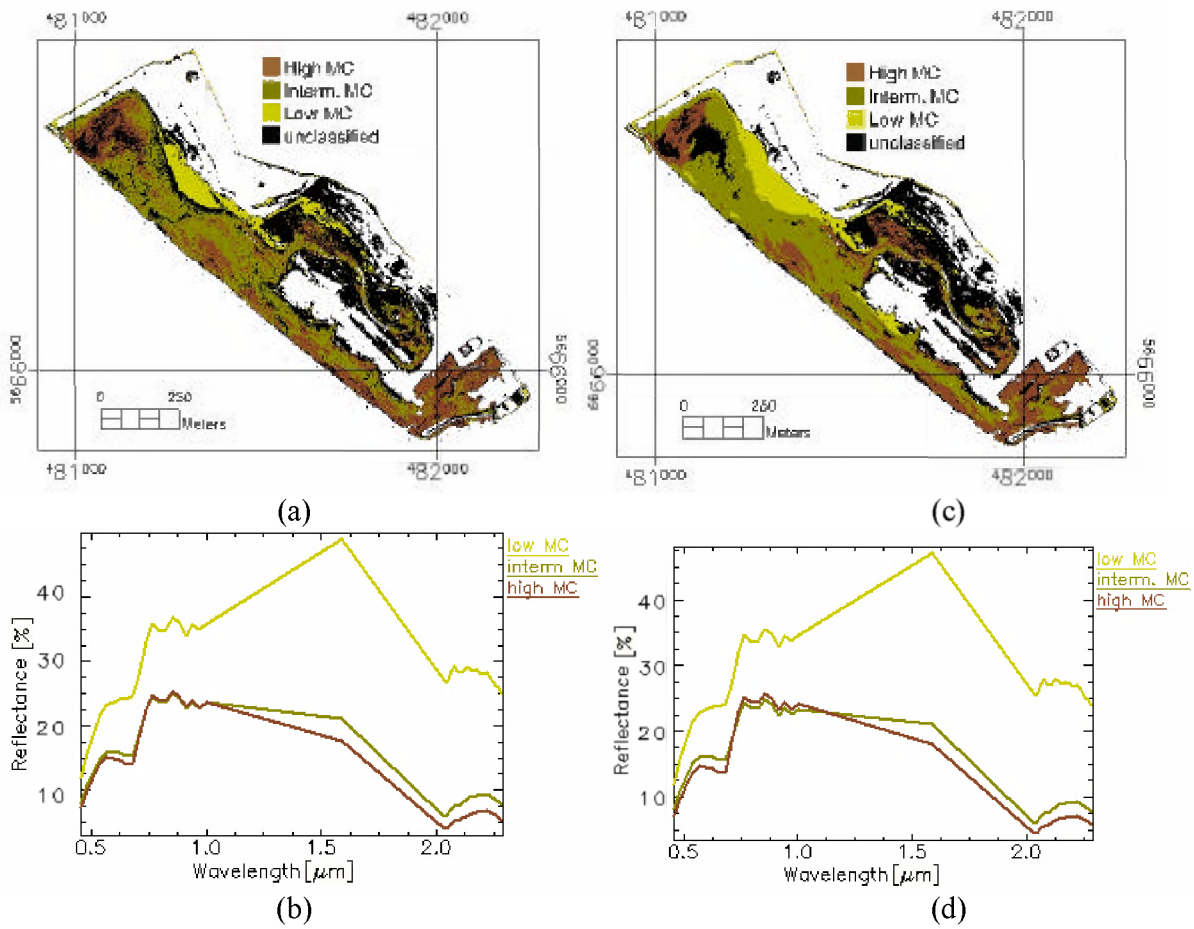

Figure 3.22: Classification results and mean spectra for IJ_AHS_07 – MC with a threshold angle of 0.10 radians (a) and (b) all bands; (c) and (d) five bands

Table 3.12: Classification accuracy results IJ_AHS_07 – MC

threshold angle (radians)	Features	classification accuracy (%) and the number of unclassified locations			
		3x3 pixels	unclassified locations	central pixel	unclassified locations
0.1	all bands	17	10	48	3
0.1	five bands	39	2	65	1

iii. BPC

Due to format incompatibility between the BPC code and the AHS image, it is not possible to have a classification for MC

3.2.3 Mud content

i. Reference and training data

To categorize mud content, three classes were identified, low MUC (5 sampling sites), intermediate MUC (12 sampling sites), and high MUC (14 sampling sites). Each sampling sites were referred to as 3×3 pixels used as reference data for the classification, leading to 279 reference pixels. Figure 3.23 the mean spectra corresponding to the reference pixels of each class.

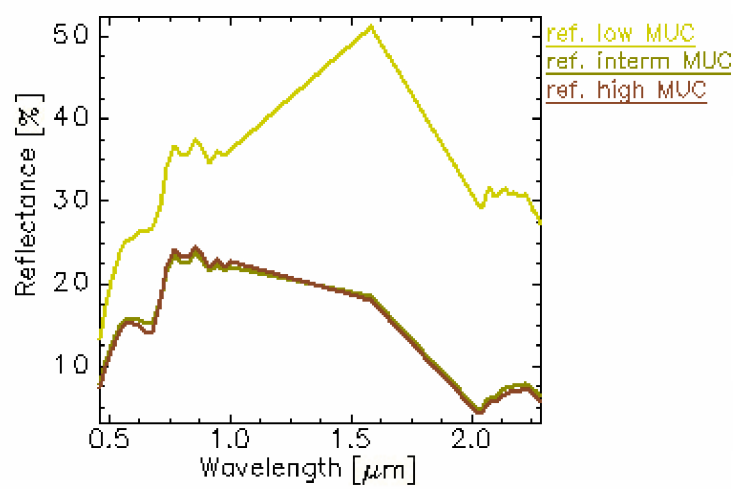

Figure 3.23: Mean spectra of reference pixels for each class (IJ_AHS_07)

ii. SAM

To classify the whole image, a threshold angle of 0.30 radians was required while using all the bands or five bands (Table 3.10) respectively. Figure 3.24 shows the classification results. Table 3.13 shows the classification accuracies obtained for the results.

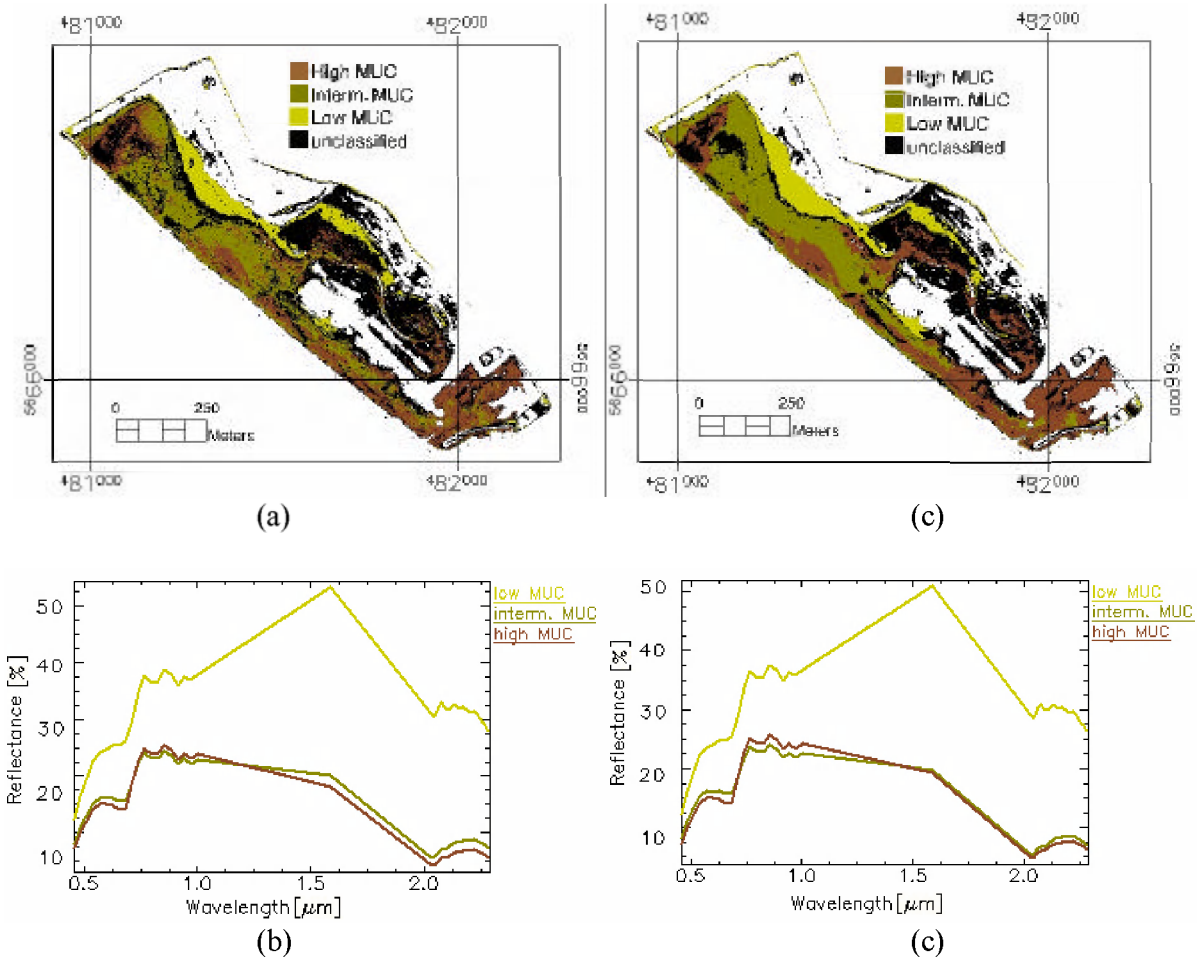

Figure 3.24: Classification results and mean spectra for IJ_AHS_07 – MUC with a threshold angle of 0.10 radians
(a) and (b) all bands; (c) and (d) five bands

Table 3.13: Classification accuracy results IJ_AHS_07 – MUC

threshold angle (radians)	Features	classification accuracy (%) and the number of unclassified locations			
		3x3 pixels	unclassified locations	central pixel	unclassified locations
0.1	all bands	19	10	56	6
0.1	five bands	52	3	68	5

iii. BPC

Due to format incompatibility between the BPC code and the AHS image, it is not possible to have a classification for MUC.

3.2.4 Discussion and conclusions

From the above results, a confirmation of the correlation between the properties is again noticed. For example, it can be seen that the areas where high chl *a* is present, the mud content, and moisture content are relatively high.

The mean spectra of the reference pixels and the classification results are quite comparable. The use of threshold angles of 0.10 radians indicates high similarity between the classified pixels. Yet, when referring to the field data for the classification accuracy, it was generally quite low due to the low number of field data, and to the fact that many of the reference pixels were "unclassified" with an angle of 0.10 radians.

A comparison was drawn between SAM classifications using all the bands versus SAM classifications using only five bands. It can be seen that the two methodologies require the same threshold angle to classify a similar area of the image. Comparing the results obtained by all the bands to the results obtained by using five bands, they were quite similar, either by referring to the classification results or the classification accuracy (Figure 3.20, Figure 3.22, and Figure 3.24). There was no classification carried out by Binary Pairwise Classifier due to technical difficulties.

3.3 2007 – CASI

The image was taken on the 12th June 2007. It was received as three individual tracks and therefore, the fist step was to mosaic the image. Yet, due to various shifts in the image, the individual tracks were relatively of different reflectance values. This was problematic for the classification. Therefore, this image was not classified. Figure 3.25 shows a quicklook of the mosaicked image.

Figure 3.25: CASI 2007 preview

4 Results: Molenplaat

4.1 2004 – HYMAP

This image was taken on the 8th June, 2004 at low tidal conditions. The flight campaign was between 13:22 and 14:41 local time and low tide occurred at 14:42 local time. The image has a 4 m × 4 m pixel size and has various unusable bands in the SWIR region. It contains 128 spectral bands from which 126 non-corrupt bands are used covering the VNIR and SWIR parts of the spectrum. Prior to classification, water was masked out of the image. The properties sampled in the corresponding field campaign are MC, MUC, chl *a* content, and organic matter content. Figure 4.1 shows the distributions of these properties in the field data. The number of observations for each property was: 73 for MC and 74 for MUC, OM, and chl *a* content. The image is classified by BPC using feature selection and SAM using all bands and only the five bands shown in Table 4.1.

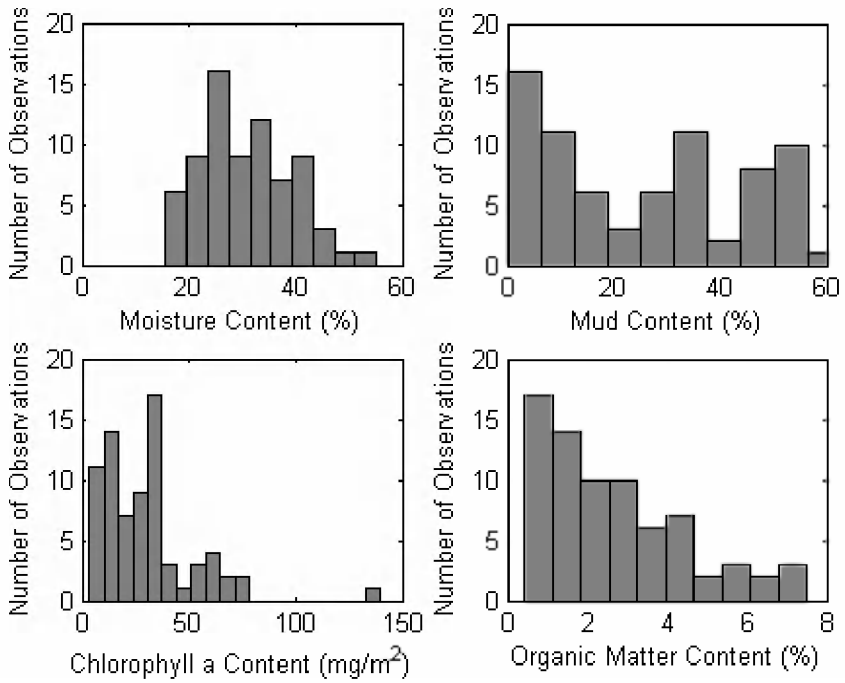

Figure 4.1: Sediment property distributions based on 2004 field measurements on the Molenplaat

Table 4.1: The five selected bands from the MO_HYMAP_04 image

band	Wavelength (nm)	FWHM (nm)
4	482	16
8	543	16
15	650	15
33	912	17
74	558	15

4.1.1 Chl *a*

i. Reference and training data

Only two classes were identified, low (12 sampling sites) and intermediate chl *a* (1 sampling site) leading to 117 reference pixels. Figure 4.2 shows the mean spectra of these reference pixels.

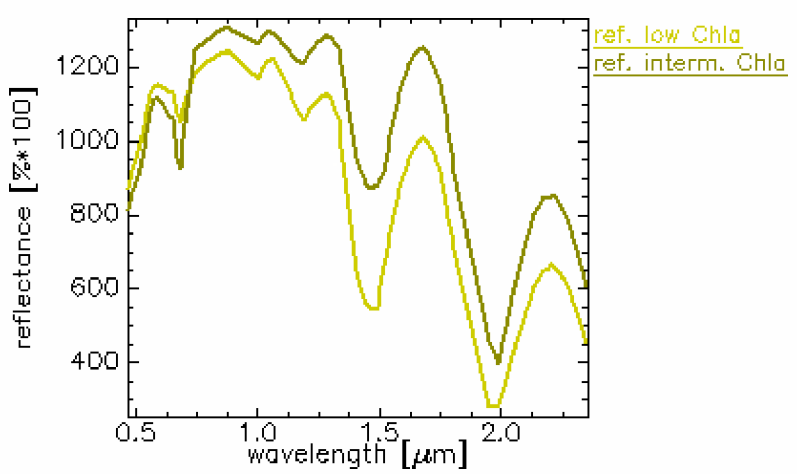

Figure 4.2: Mean spectra of reference pixels for each class (MO_HYMAP_04)

ii. SAM

To classify the whole image, angles of 0.5 and 0.3 radians were required while using all the bands or five bands respectively (Table 4.1). Figure 4.3 and Table 4.2 show the results.

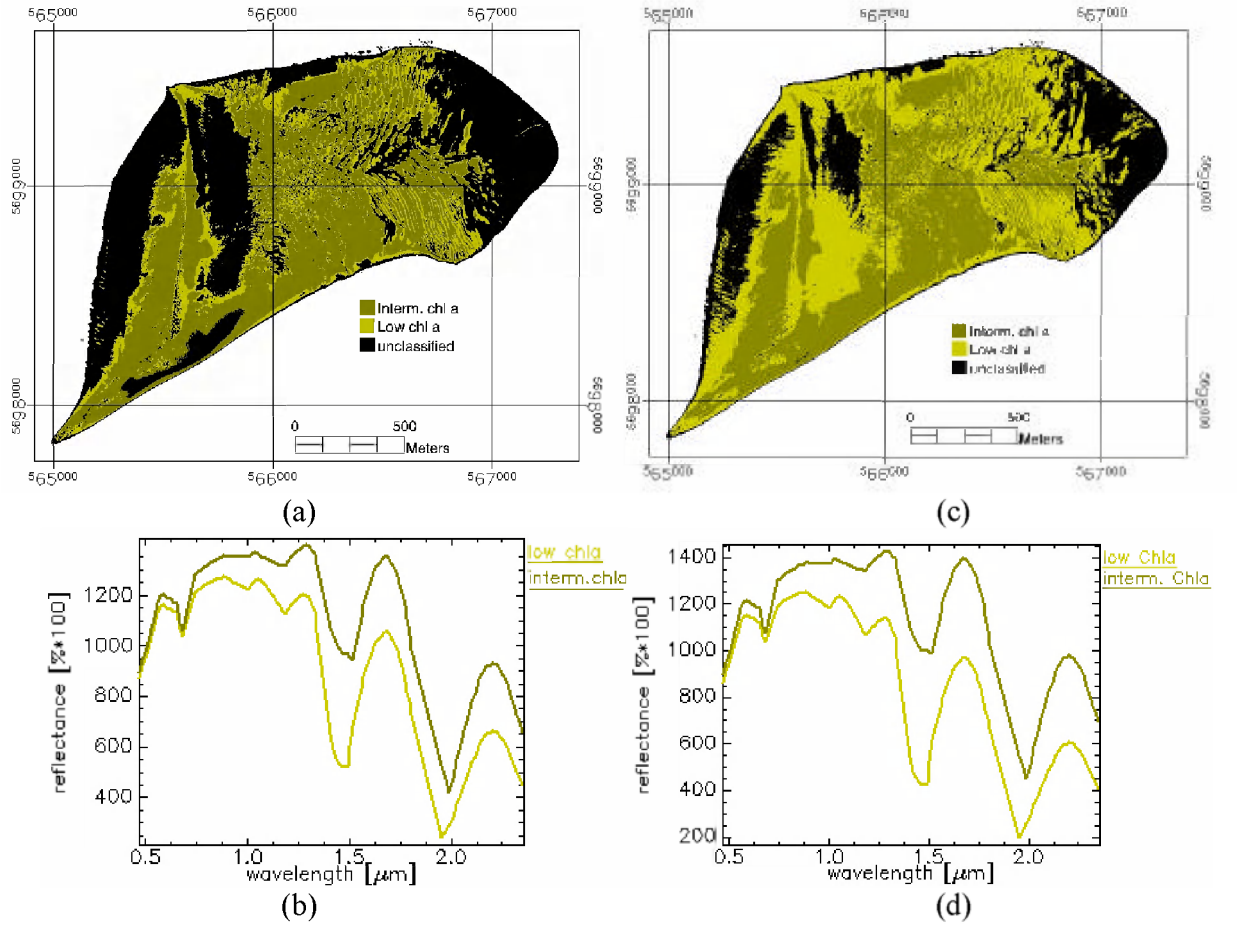

Figure 4.3: Classification results and mean spectra for MO_HYMAP_04 – chl *a* with a threshold angle of 0.10 radians
(a) and (b) all bands; (c) and (d) five bands

Table 4.2: Classification accuracy results MO_HYMAP_04 – chl *a*

threshold angle (radians)	Features	classification accuracy (%) and the number of unclassified locations			
		3x3 pixels	unclassified locations	central pixel	unclassified locations
0.1	all bands	0	5	20	2
0.1	five bands	40	3	47	2

iii. BPC

To classify chl *a*, 50% of the available data were used for training and the remaining 50% were used for validation. The classification was carried out ten times where for each run, a random choice of training and validation pixels was done. The average validation accuracy of the ten runs was 76 % with a standard deviation of 20 %. The run with the highest accuracy of 100 % resulted in the classified image shown in Figure 4.4. Table 4.3 shows the features selected to discriminate a pair of classes.

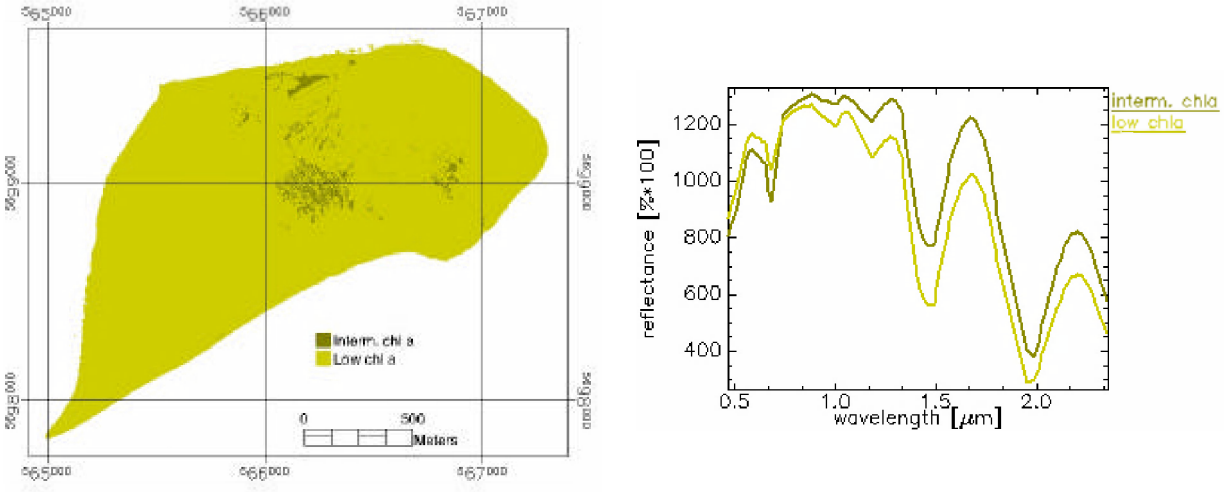

Figure 4.4: Classification results and mean spectra for MO_HYMAP_04 – chl *a*

Table 4.3: The results of feature selection for each pair of classes (MO_HYMAP_04 - chl *a*)

Class (1)	Class (2)	Number of features selected	Features
Low chl *a*	Interm. chl *a*	2	18(695), 19(740)

4.1.2 Moisture Content

i. Reference and training data

To categorize moisture content, three classes were identified, low (1 sampling site), intermediate (17 sampling sites), and high (2 sampling sites) Each sample was used as 3×3 pixels and utilized as reference data for the classification, leading to 180 reference pixels. Figure 3.23 shows the mean spectra corresponding to the reference pixels of each class.

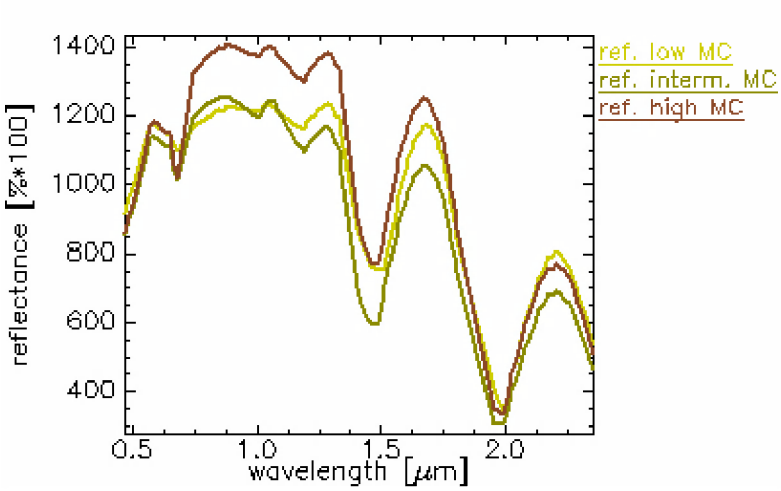

Figure 4.5: Mean spectra of reference pixels for each class (MO_HYMAP_04)

ii. SAM

To classify the whole image, angles of 0.5 and 0.3 radians were required while using all the bands or five bands (Table 4.1) respectively. Figure 4.6 shows the classification results with an angle of 0.10 radians. Table 4.4 shows the classification accuracies obtained for the results.

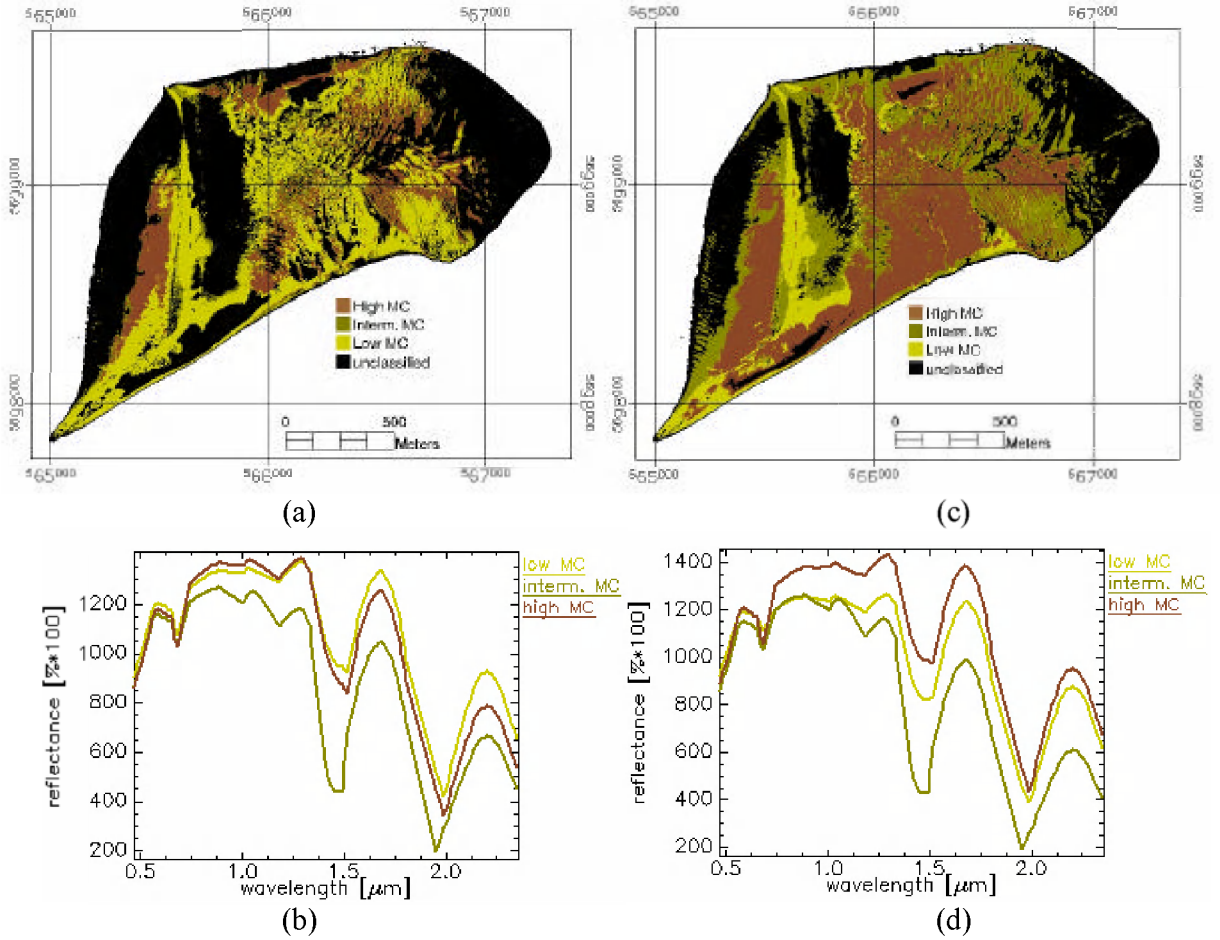

Figure 4.6: Classification results and mean spectra for MO_HYMAP_04–MC with a threshold angle of 0.10 radians
(a) and (b) all bands; (c) and (d) five bands

Table 4.4: Classification accuracy results MO_HYMAP_04 – MC

threshold angle (radians)	Features	classification accuracy (%) and the number of unclassified locations			
		3x3 pixels	unclassified locations	central pixel	unclassified locations
0.1	all bands	5	6	20	5
0.1	five bands	25	3	35	3

iii. BPC

To classify moisture content, 50 % the available data were used for training and the remaining data were used for validation. The classification was carried out ten times where for each run, a random choice of training and validation pixels was done. The average validation accuracy of the ten runs was 47 % with a standard deviation of 15 %. The run with the highest accuracy of 71 % resulted in the classified image shown in Figure 4.7. Table 4.5 shows the features selected to discriminate a pair of classes.

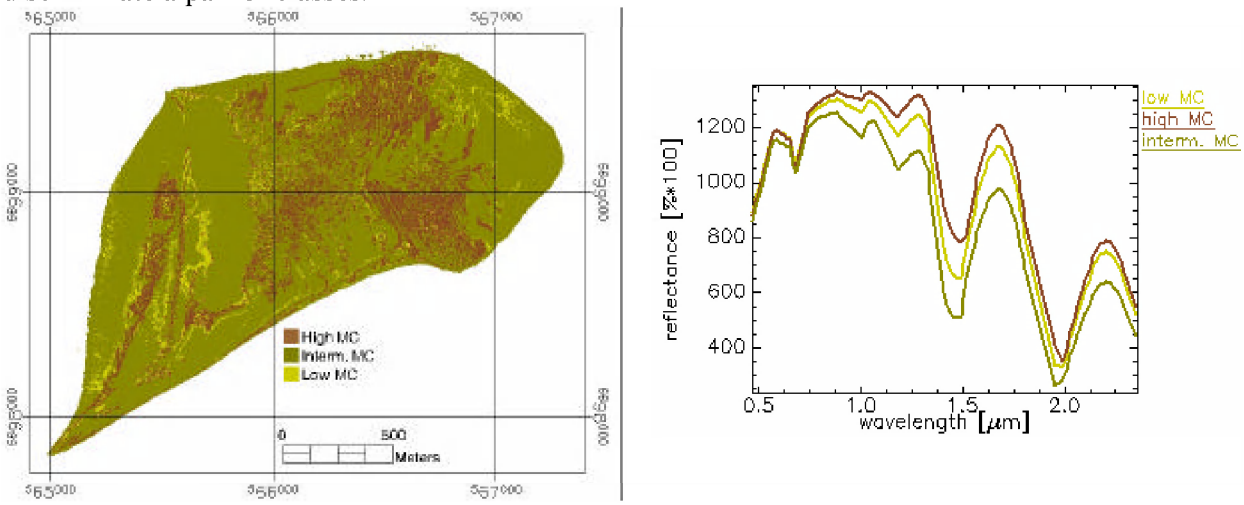

Figure 4.7: Classification results and mean spectra for MO_HYMAP_04 – moisture content

Table 4.5: The results of feature selection for each pair of classes (MO_HYMAP_04 – moisture content)

Class (1)	Class (2)	Number of features selected	Features
Low MC	High MC	1	14(665)
Low MC	Interm. MC	1	19(740)
high MC	Interm. MC	1	99(2065)

4.1.3 Mud content

i. Reference and training data

To categorize mud content, three classes were identified, low MUC (7 sampling site), intermediate MUC (6 sampling site), and high MUC (6 sampling site). Each sample was used as 3×3 pixels as reference data for the classification, leading to 171 reference pixels.

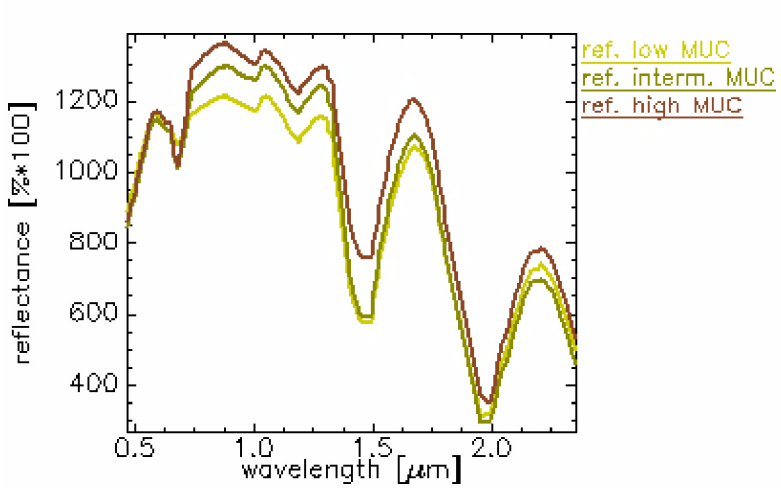

Figure 4.8: Mean spectra of reference pixels for each MUC class (MO_HYMAP_04)

ii. SAM

To classify the whole image, angles of 0.5 and 0.3 radians were required while using all the bands or five bands (Table 4.1) respectively. Figure 4.9 shows classification results with an angle of 0.10 radians. Table 4.6 shows the classification accuracies obtained for the results.

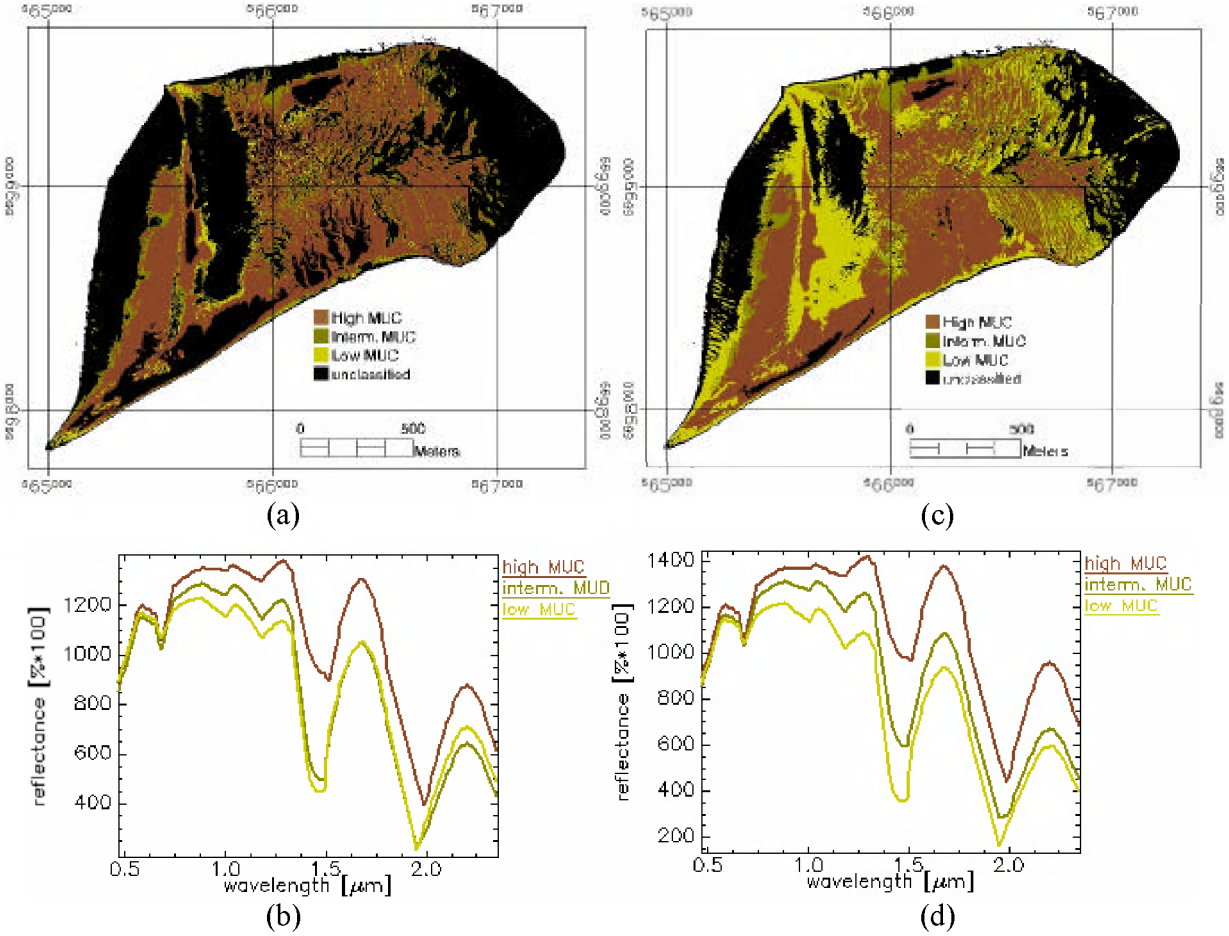

Figure 4.9: Classification results and mean spectra for MO_HYMAP_04 – MUC with a threshold angle of 0.10 radians
(a) and (b) all bands; (c) and (d) five bands

Table 4.6: Classification accuracy results MO_HYMAP_04 – MUC

threshold angle (radians)	Features	classification accuracy (%) and the number of unclassified locations			
		3x3 pixels	unclassified locations	central pixel	unclassified locations
0.1	all bands	32	2	47	2
0.1	five bands	32	3	53	3

iii. BPC

To classify mud content, 40, 50, 60, or 70 % of the available data were used for training and the remaining was used for validation. The classification was carried out ten times for each partition of the data; where for each run, a random choice of training and validation pixels was done. Yet, it was not possible to classify this image by the BPC code. This is due to the fact that the number of reference field samples used for training is relatively small with respect to the dimensionality of the data. This leads to difficulties in estimate class pdfs for each class.

4.1.4 Organic matter

i. Reference and training data

To categorize OM, only two classes were identified, low (13 sampling sites) and intermediate (1 sampling site). Each sample was 3×3 pixels and used as reference data for the classification, leading to 126 reference pixels.

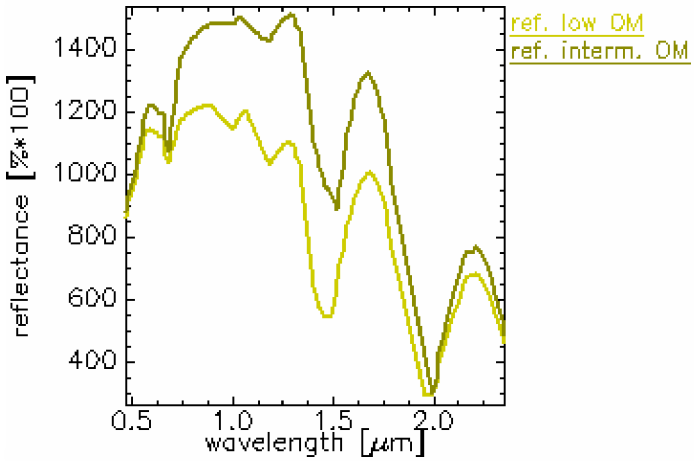

Figure 4.10: Mean spectra of reference pixels for each OM class (MO_HYMAP_04)

ii. SAM

To classify the whole image, angles of 0.5 and 0.3 radians were required while using all the bands or five bands (Table 4.1) respectively. Figure 4.11 shows the classification results of a threshold angle of 0.10 radians. Table 4.7 shows the classification accuracies obtained for the results.

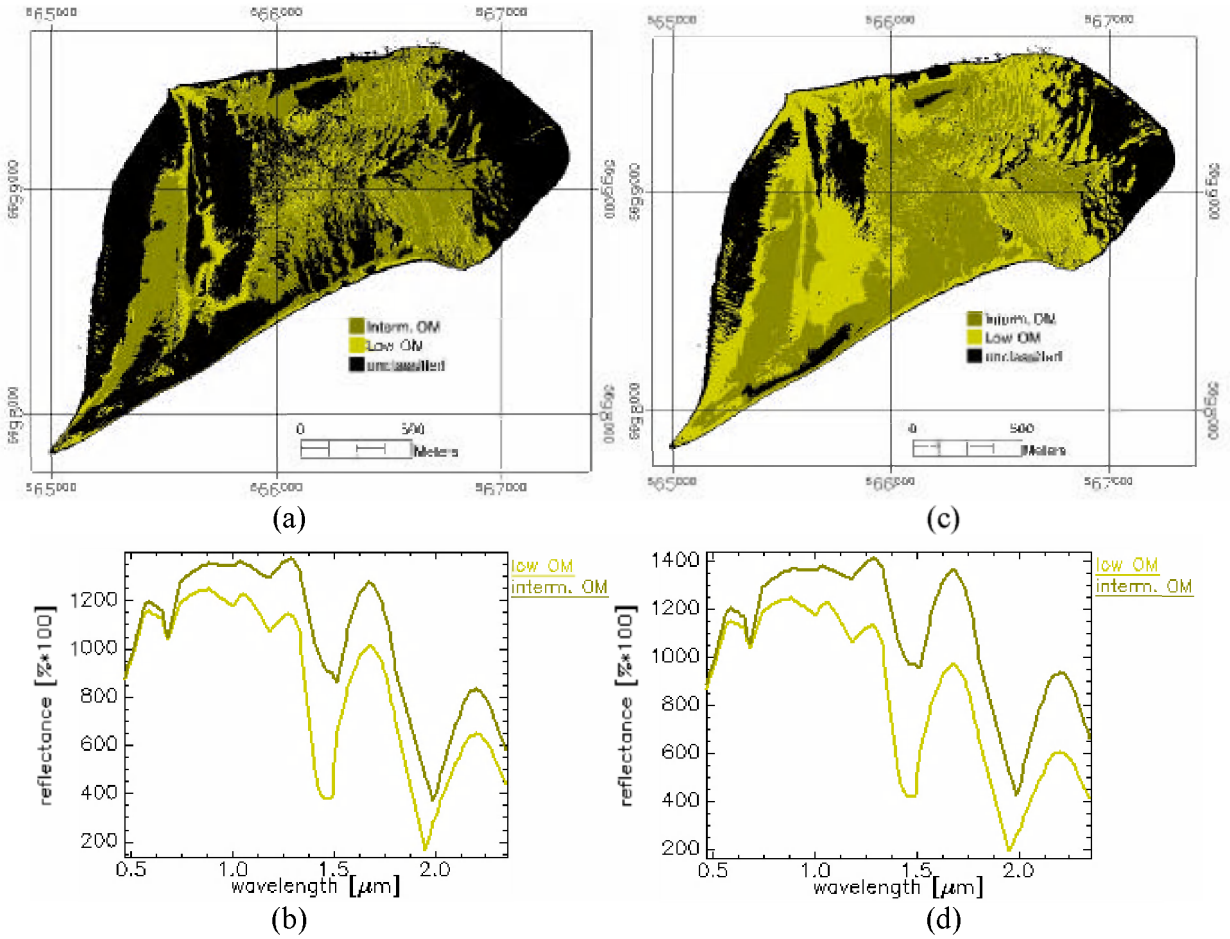

Figure 4.11: Classification results and mean spectra for MO_HYMAP_04 – OM with a threshold angle of 0.10 radians
(a) and (b) all bands; (c) and (d) five bands

Table 4.7: Classification accuracy results MO_HYMAP_04 – OM

threshold angle (radians)	Features	classification accuracy (%) and the number of unclassified locations			
		3x3 pixels	unclassified locations	central pixel	unclassified locations
0.1	all bands	14	6	14	6
0.1	five bands	21	2	43	2

iii. BPC

To classify organic matter, 50 % of the available data were used for training and the remaining data were used for validation. The classification was carried out ten times where for each run, a random choice of training and validation pixels was done. The average validation accuracy of the ten runs was 77 % with a standard deviation of 15 %. The run with the highest accuracy of 86 % resulted in the following (Figure 4.12 and Table 4.8):

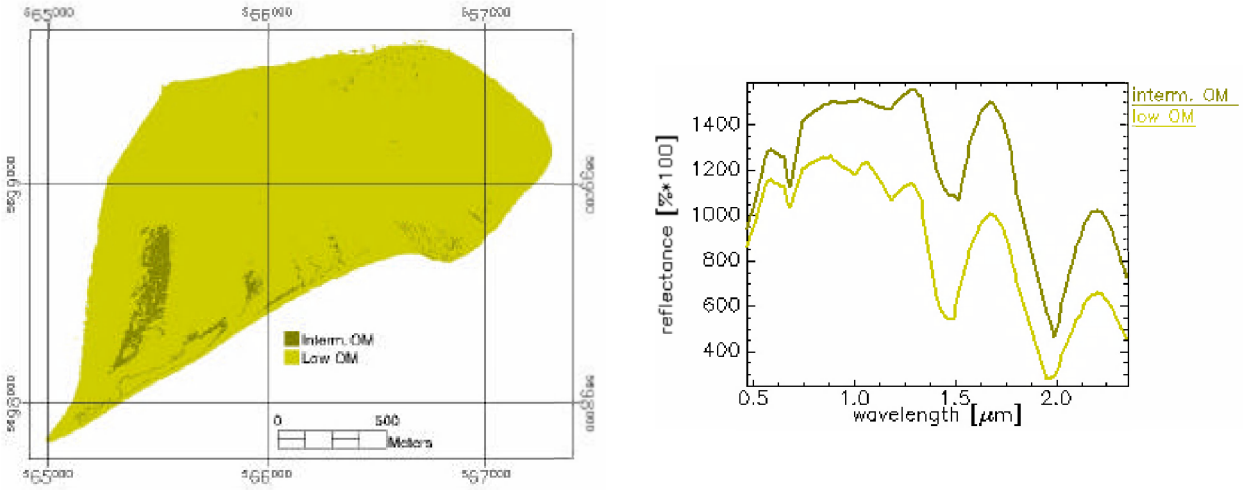

Figure 4.12: Classification results and mean spectra for MO_HYMAP_04 – organic matter content

Table 4.8: The results of feature selection for each pair of classes (MO_HYMAP_04 – organic matter content)

Class (1)	Class (2)	Number of features selected	Features
Low OM	Interm. OM	1	30(896)

4.1.5 Discussion and conclusions

i. A discussion of the different results

By observing the results, the correlation between the properties is noticed again. It can be also seen that a threshold angle of 0.10 radians lead to more classified areas when only the five bands were used. When referring to the field data for the classification accuracy, it is generally quite low. It must be noted that the number of field data is again too low to reach a comprehensive conclusion. The values of classification accuracy of BPC are relatively high. Yet, similarly to SAM, the number of field data used is too low to result in a comprehensive overview of the classification accuracy.

For chl *a*, the mean spectra of the results of SAM (Figure 4.3) do not resemble the reference spectra (Figure 4.2), especially in the aspect of the chl *a* dip. Yet, the BPC results lead to mean spectra that show similar behavior to the reference spectra (Figure 4.4). For moisture content, the mean spectra of the results of SAM (Figure 4.6) do not resemble the reference spectra (Figure 4.5). For mud content and organic matter content, the mean spectra of the results resemble the reference spectra (Figure 4.8, Figure 4.9, Figure 4.10, Figure 4.11, Figure 4.12, and Figure 4.13).

A comparison was drawn between SAM and BPC. For chl *a* content, the results of BPC showed more dominance of low chl *a* areas (Figure 4.3 and Figure 4.4). Regarding moisture content, the results of the BPC showed more dominance to intermediate MC (Figure 4.6 and Figure 4.7). Finally, BPC showed more dominance to low OM (Figure 4.11and Figure 4.12).

The feature selection carried out while applying the BPC resulted in specific bands used to classify the different properties. It can be seen that a SWIR band was only used to differentiate the different classes of MC (Table 4.5).

ii. A comparison to previous work

In the work of Adam et al. (2006), this HYMAP image of the Molenplaat was classified by SAM with a threshold angle of 0.10 radians. Yet, a different approach was used for the classification. First, different thresholds for each property were used to make each class since they

considered only one field campaign on one study area. Second, the classification was not carried for each individual property, but rather for different "Groups", where each group represented a combination to different properties. Therefore, a direct comparison cannot be carried out between the results, and classification accuracy values in one, is not comparable to the other. Yet, the resulting classes can be traced back in all the results. Furthermore, the unclassified areas, especially when only the five chosen bands are used.

In the work of Deronde et al. (2006), the same image was also classified. Similarly to the work in this report, the classification was carried out per individual property, yet with different classes for each property. Therefore, a direct comparison of classification accuracy is also not valid. Yet, the patterns in the resulting classes can be compared. The comparison showed a similarity in the results, especially for the classification of chl *a* content.

4.2 2005 - AHS

This image was taken on the 23rd June, 2005 at low tidal conditions. The flight campaign was between around 15:36 local time and low tide occurred at 17:26 local time. The image has a 4.371 m × 4.708 m and contains 21 usable bands covering the VNIR and SWIR parts of the spectrum. Prior to classification, water was masked out of the image. The properties sampled in the corresponding field campaign were chl *a* and mud content. Figure 4.13 shows the distribution of these properties in the field data. The number of observations was 52 for chl *a* content and 62 for MUC.

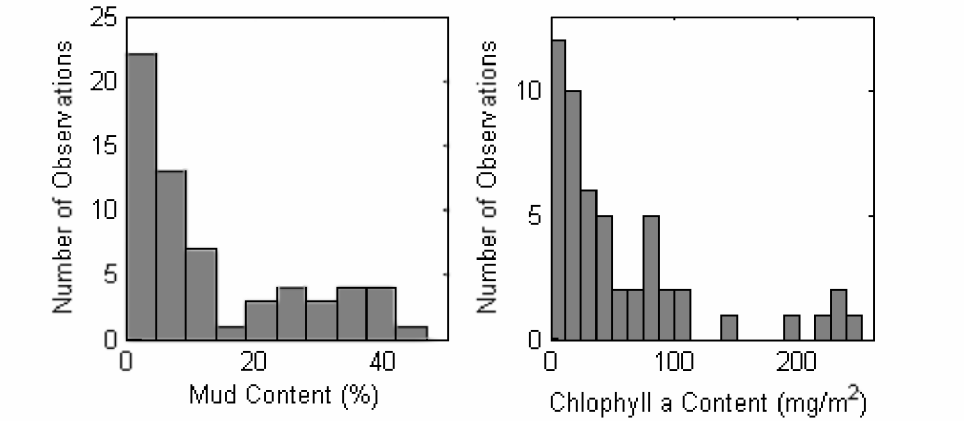

Figure 4.13: Sediment property distributions based on 2005 field measurements on the Molenplaat

The image is classified by BPC using feature selection and SAM using all bands and only the five bands shown in Table 4.9.

Table 4.9: The five selected bands from MO_AHS_05 image

band	Wavelength (nm)	FWHM (nm)
1	455	27
4	542	28
8	659	28
17	918	28
21	1622	159

4.2.1 Chl *a*

i. Reference and training data

To categorize chl *a*, three classes were identified, low (13 sampling locations) and intermediate chl *a* (1 sampling location). Each sample, as 3 × 3, pixels was used as reference data for the classification, leading to 126 reference pixels.

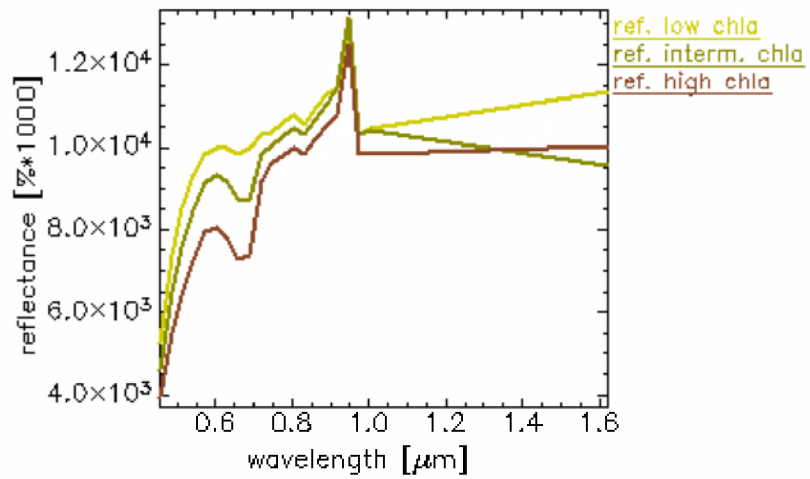

Figure 4.14: Mean spectra of reference pixels for each class (MO_AHS_05)

ii. SAM

To classify the whole image, an angle of 0.30 radians was required while using all the bands or five bands (Table 4.9). Figure 4.15 and Figure 4.16 show the classification results with an angle of 0.10 and 0.20 radians. Table 4.10 shows the classification accuracies obtained for the results.

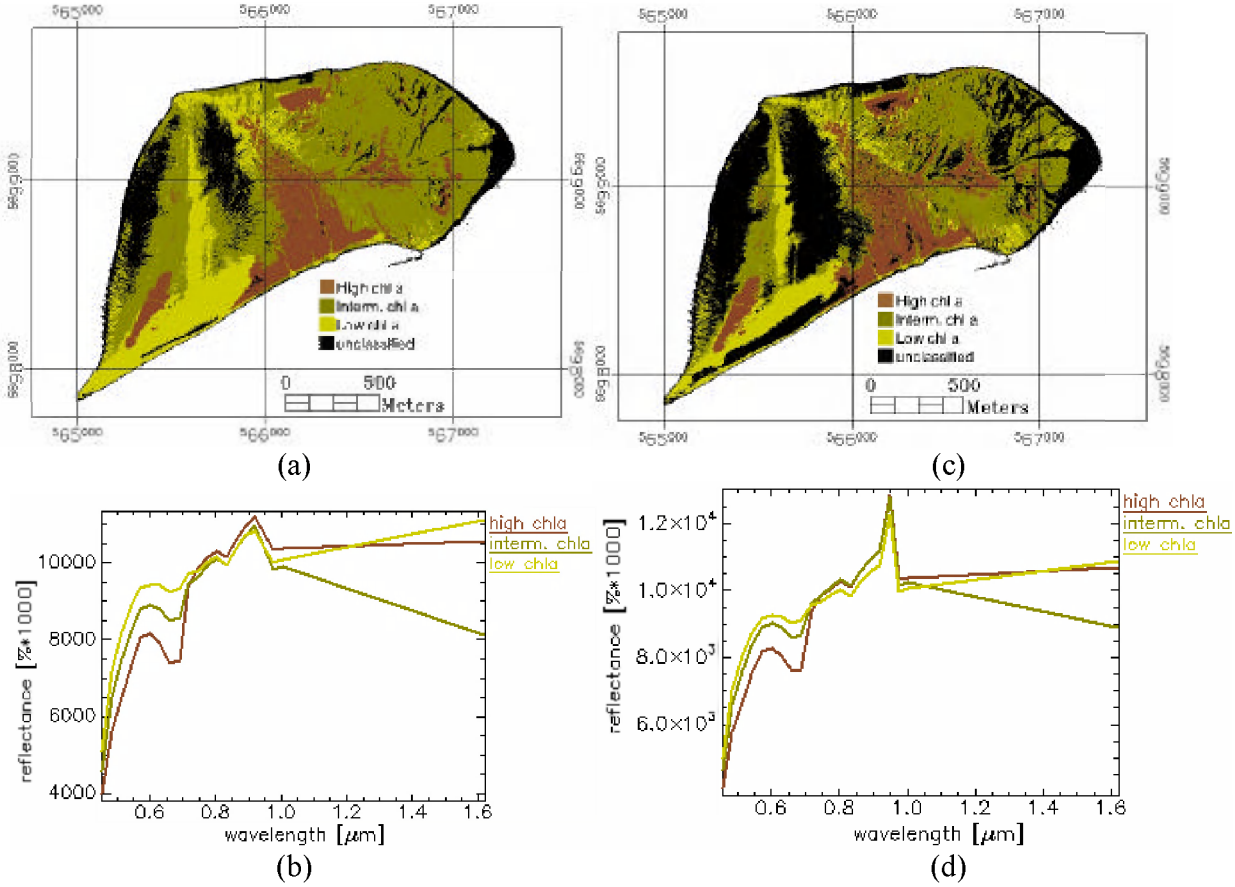

Figure 4.15: Classification results and mean spectra for MO_AHS_05 – chl *a* with a threshold angle of 0.10 radians
(a) and (b) all bands; (c) and (d) five bands

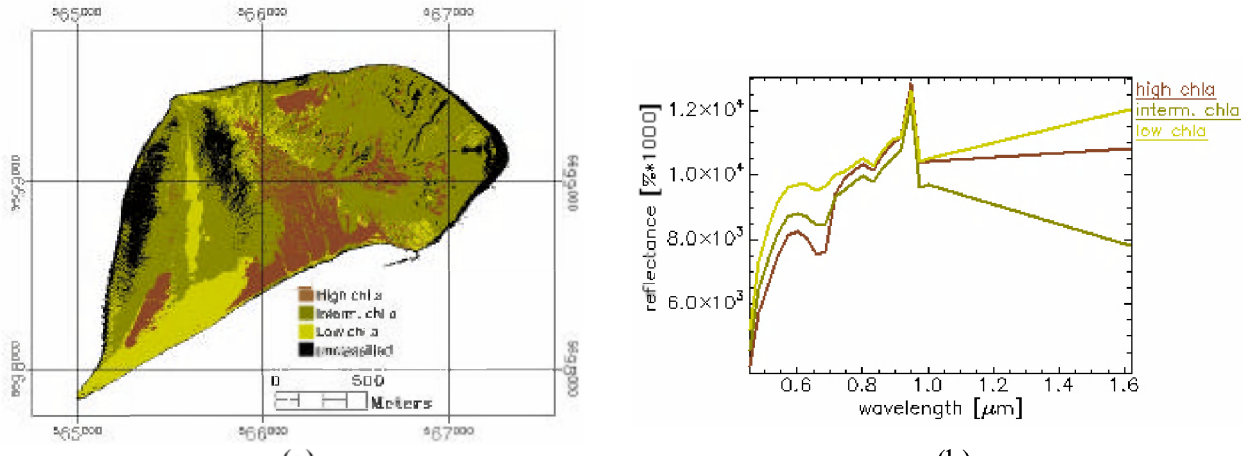

(a) (b)

Figure 4.16: Classification results and mean spectra for MO_AHS_05 chl *a* with a threshold angle of 0.20 radians and five band selection

Table 4.10: Classification accuracy results MO_AHS_05 – chl *a*

threshold angle (radians)	Features	classification accuracy (%) and the number of unclassified locations			
		3x3 pixels	unclassified locations	central pixel	unclassified locations
0.1	all bands	55	2	55	2
0.1	five bands	27	3	55	2
0.2	five bands	46	0	73	0

iii. BPC

To classify chl *a*, 55% of the available data were used for training and the remaining 45% were used for validation. The classification was carried out ten times where for each run, a random choice of training and validation pixels was done. The average validation accuracy of the ten runs was 57 % with a standard deviation of 6 %. The run with the highest accuracy of 64 % resulted in the classified image shown in Figure 4.17. Table 4.11 shows the features selected to discriminate each pair of classes.

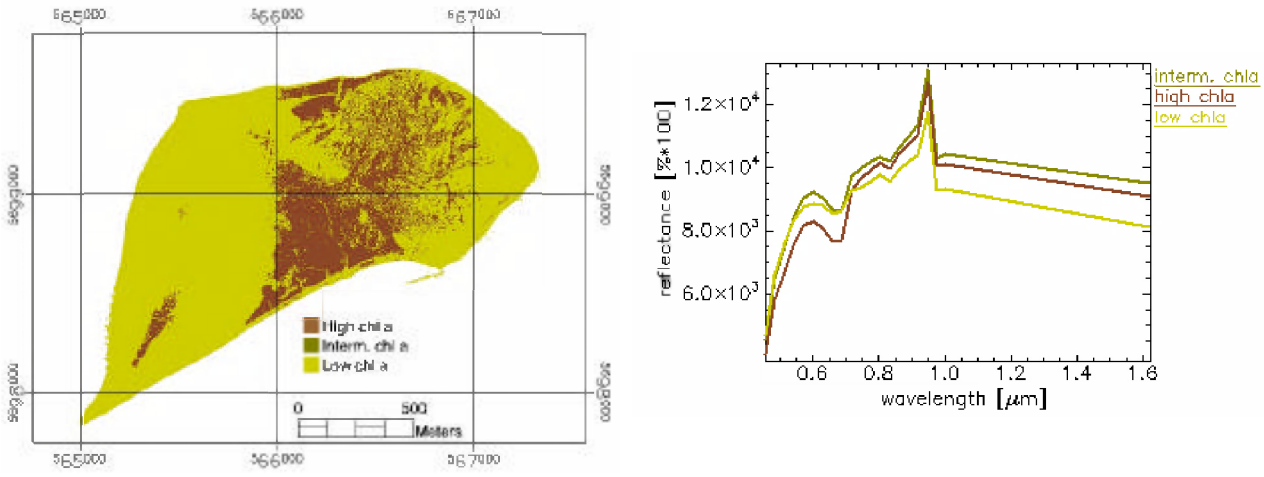

(a) (b)

Figure 4.17: Classification results obtained for MO_AHS_05 - chl *a*

Table 4.11: The results of feature selection for each pair of classes (MO_AHS_05 - chl *a*)

Class (1)	Class (2)	Number of features selected	Features
Low chl *a*	Interm. chl *a*	3	20(1004),7(630),18(948)
Low chl *a*	High. chl *a*	3	1(455)
Interm. chl *a*	High chl *a*	4	1(455),13(804),6(601),8(659)

4.2.2 Mud content

i. Reference and training data

To categorize mud content, three classes were identified, low MUC (8 samples), intermediate MUC (5 samples), and high MUC (1 sample). Each sample was used as 3 × 3 pixels used as reference data for the classification, leading to 126 reference pixels.

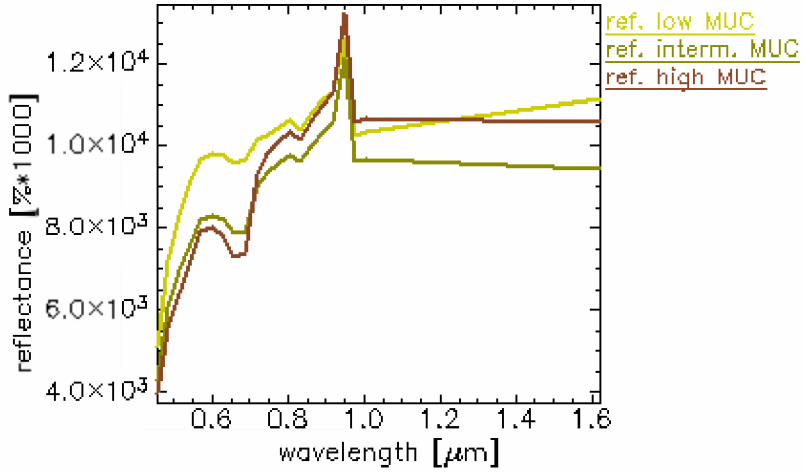

Figure 4.18: Mean spectra of reference pixels for each class (MO_AHS_05)

ii. SAM

To classify the whole image, an angle of 0.3 radians was required while using all the bands or five bands (Table 4.9). Figure 4.19 and Figure 4.20 show the classification results with threshold angles of 0.10 radians and 0.2 radians. Table 4.12 shows the classification accuracies obtained for the results.

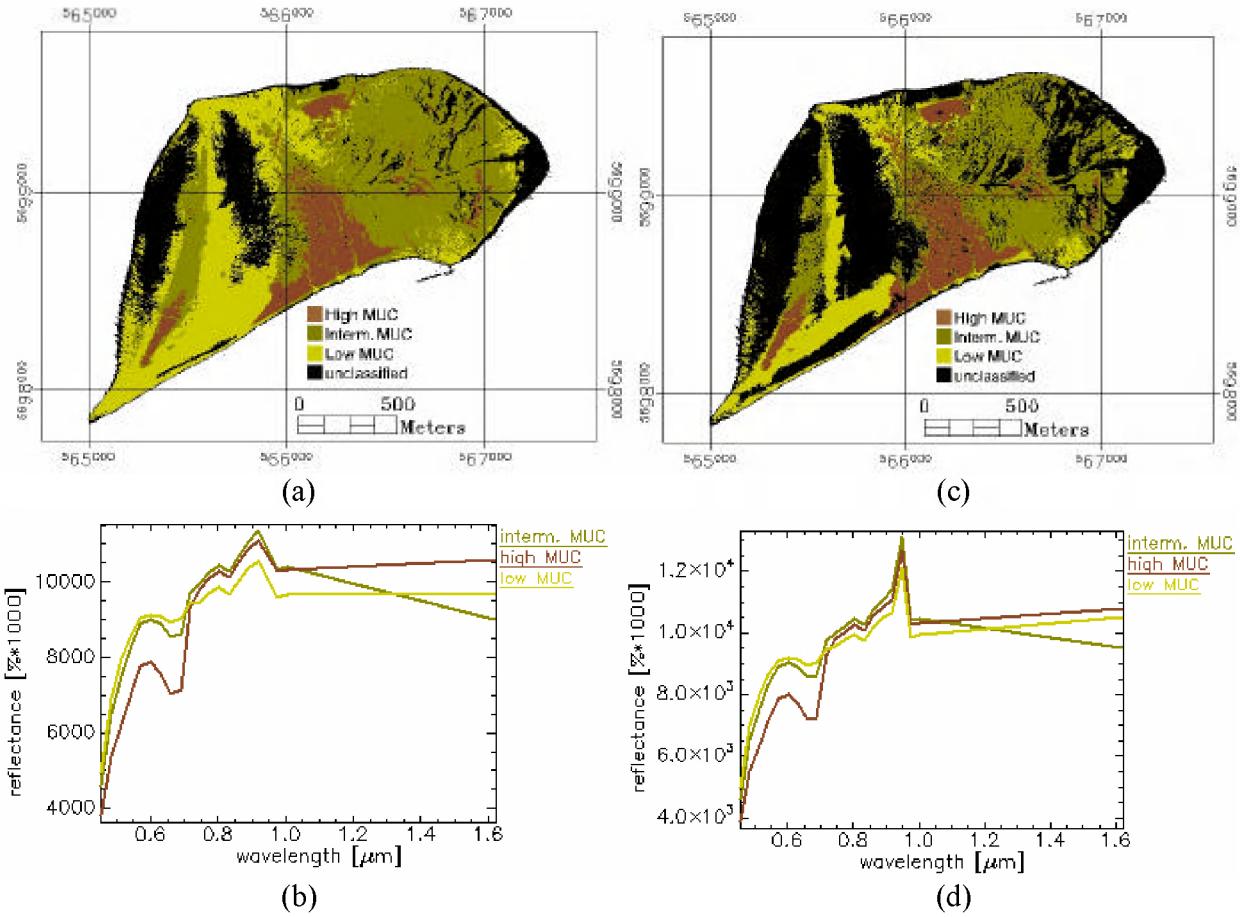

Figure 4.19: Classification results and mean spectra for MO_AHS_05 – chl *a* with a threshold angle of 0.10 radians
(a) and (b) all bands; (c) and (d) five bands

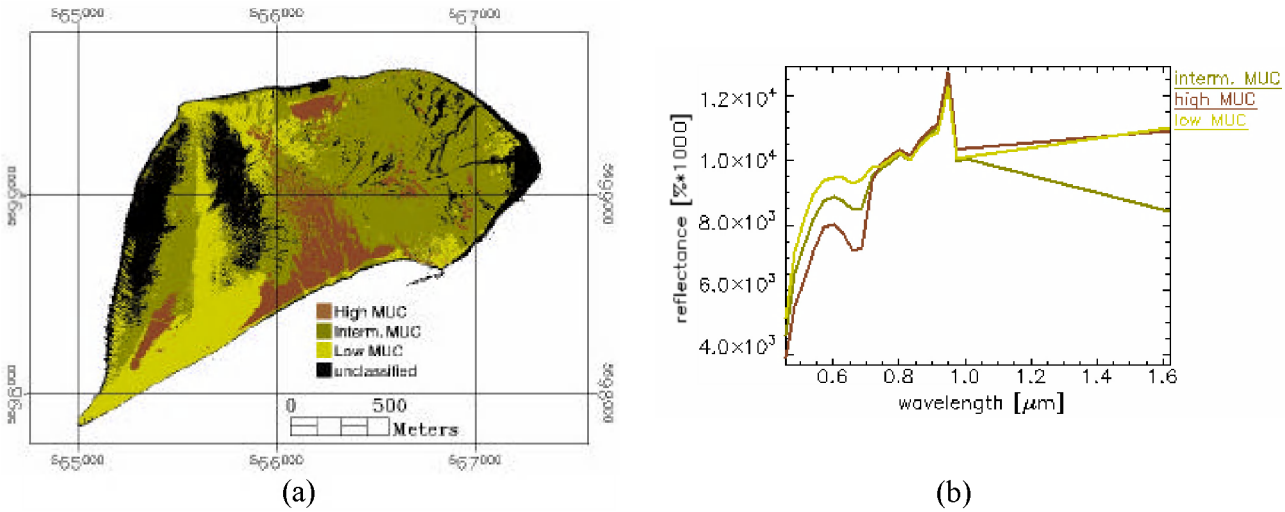

Figure 4.20: Classification results and mean spectra for MO_AHS_05 MUC with a threshold angle of 0.20 radians and five band selection

Table 4.12: Classification accuracy results MO_AHS_05 – MUC

threshold angle (radians)	Features	classification accuracy (%) and the number of unclassified locations			
		3x3 pixels	unclassified locations	central pixel	unclassified locations
0.1	all bands	71	6	71	2
0.1	five bands	36	6	71	2
0.2	five bands	57	1	71	1

iii. BPC

To classify mud content, 50% of the available data were used for training and the remaining data were used for validation. The classification was carried out ten times where for each run, a random choice of training and validation pixels was done. The average validation accuracy of the ten runs was 74% with a standard deviation of 14%. The run with the highest accuracy of 92% resulted in the following (Figure 4.21 and Table 4.13):

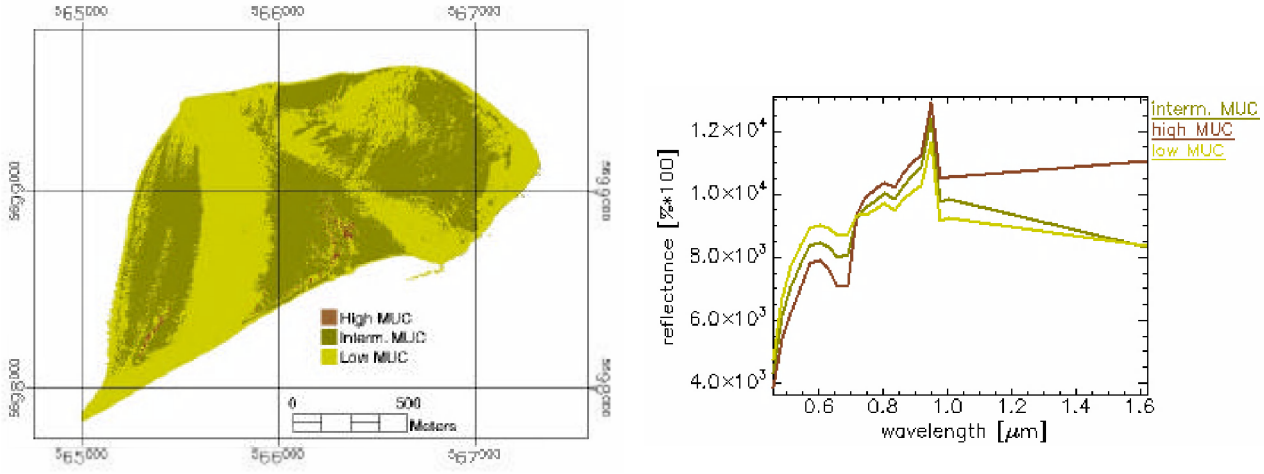

(a) (b)

Figure 4.21: Classification results obtained for AHS 2005 - MUC

Table 4.13: The results of feature selection for each pair of classes (AHS 2005 – mud content)

Class (1)	Class (2)	Number of features selected	Features
Low MUC	Interm. MUC	5	6(601),17(918),7(630),13(804),3(513)
Low MUC	High MUC	2	10(718),15(862)
Interm. MUC	High MC	2	12(774), 6(601)

4.2.3 Discussion and conclusions

The correlation between the properties was noted again. It can be also seen that a threshold angle of 0.10 radians with five bands (Table 4.9) lead to more classified areas when all the bands were used.

For chl *a*, the mean spectra of the results of resemble the reference spectra. Yet, the BPC results lead to mean spectra that do not show similar behavior to the reference spectra (Figure 4.15 Figure 4.16, and Figure 4.17). For mud content, the results of SAM using few bands and a threshold angle of 0.20 rad have the mean reference spectra that are the most similar to the reference spectra (Figure 4.19 and Figure 4.20).

When referring to the field data for the classification accuracy, it is generally quite low. It must be noted that the number of field data is again too low to reach a comprehensive conclusion. The values of classification accuracy of BPC were low for chl *a* content but quite high for MUC. Similarly to SAM, the number of field data used is too low to result in a comprehensive overview of the classification accuracy.

For chl *a* content, it can be seen that the results of the BPC showed not much presence of intermediate chl a areas (Figure 4.17). Regarding mud content, the results of the BPC showed little presence of high MUC (Figure 4.21). The feature selection carried out while applying the BPC resulted in specific bands used to classify the different properties (Table 4.16 and Table 4.17).

4.3 2007- AISA

Similarly the case of the CASI image acquired in 2007 for the IJzermonding, the AISA image has problems. The four tracks covering the Molenplaat are of various ranges of reflectance values, even after inter-track reflectance calibration. Therefore, it cannot be classified using SAM. A preview of this image is shown below.

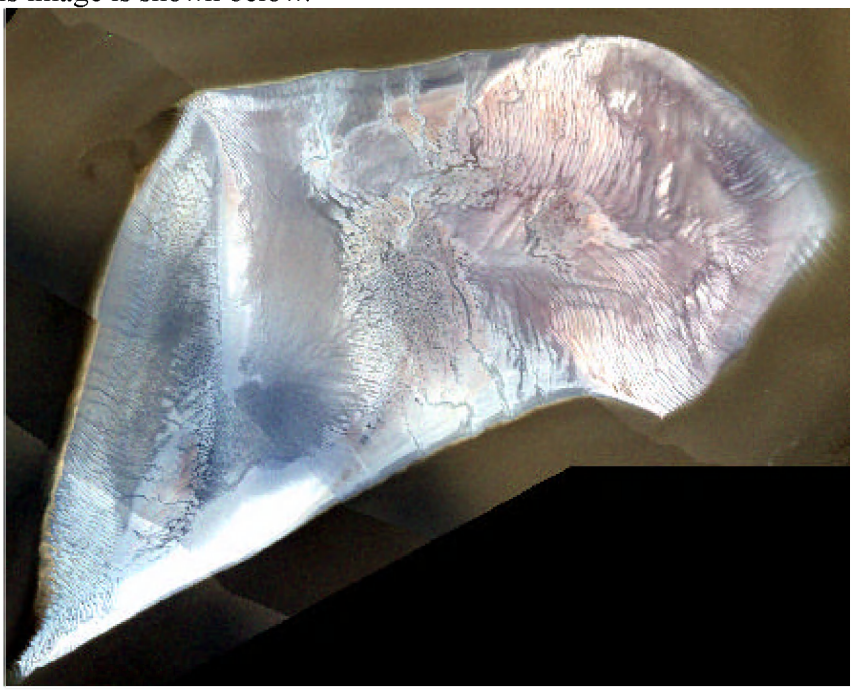

Figure 4.22: AISA 2007 preview

4.4 Conclusions

The classification accuracy of SAM using the field data showed dissimilarity between the classification of the 3×3 quadrant of pixels and the central pixels. Theoretically, this case was not expected as the field sampling locations chosen represented homogeneous areas, especially when replicates were sampled for each location. The reason for these results can be due to several uncertainties included in this type of study. For example, there were common errors with the geometric corrections of the imagery. Therefore, when the coordinates of a sampling location were located on an image, they might be shifted a few pixels (depending on the image). Furthermore, there was a discrepancy between the field sampling campaigns and flight campaigns. Since the intertidal flats are highly dynamic areas, there are a lot of changes that occur, even during the same day due to the migration of

microphytobenthos in the sediments. Therefore, what might be measured in the field might not be corresponding to what was acquired in the image, even if both occurred on the same day. The classification results of BPC also included a pair-wise feature selection. Table 4.14, Table 4.15, Table 4.16, and

Table 4.17 show the features selected to characterize each property per image. To classify chl *a*, it can be seen that no SWIR bands were used, yet bands of the blue, green, red, and NIR were utilized.

For the classification of moisture content, it can be noticed that SWIR bands were used more than for the other properties. Furthermore, green, red, and NIR were used. The Blue part of the spectrum was not used for this classification.

To classify mud content, bands of the blue, green, red, NIR, and SWIR parts of the spectrum were used.

Finally, for the classification of organic matter content, bands of the blue, red, NIR, and SWIR were used. No green bands were found useful.

Table 4.14: Features selected for the characterization of chl *a*

image	Chl a		
	low/inter	low/high	interm/high
IJ_AHS_05	455, 718, 918	689, 718, 948	455
MO_HYMAP_04	695, 740	-	-
MO_AHS_05	630, 1004, 948	455	455, 601, 659, 804

Table 4.15: Features selected for the characterization of MC

image	MC		
	low/inter	low/high	interm/high
IJ_AHS_05	513	774, 1622	513, 542, 689, 975, 1622
MO_HYMAP_04	665	740	2065
MO_AHS 05	-	-	-

Table 4.16: Features selected for the characterization of MUC

image	MC		
	low/inter	low/high	interm/high
IJ_AHS _05	455, 542, 630, 774, 1004, 1622	542, 682, 689, 1004	484, 542, 659, 689, 1004
MO_HYMAP_04	-	-	-
MO_AHS_05	513, 601, 630, 804, 918	718, 862	601, 774

Table 4.17: Features selected for the characterization of OM

image	OM		
	low/inter	low/high	interm/high
IJ_AHS_05	484, 601,689, 718, 975	630, 804, 891, 1004,	804, 891, 862, 975, 1622
MO_HYMAP_04	896	-	-
MO_AHS_05	-	-	-

5 Conclusions and recommendations

The intertidal flats are very dynamic and heterogeneous areas and require a lot more field sampling than what has been previously acquired for these images. Furthermore, in order to carry out any statistical study of the results, more data is required. Moreover, more correspondence

between the flight campaigns and the field campaigns is required. The effect of the microphytobenthic migration is also essential for this type of study. This will be taken into account in future field campaigns. In fact, this was implemented in the field campaign carried out on the IJzermonding in May 2009. Therefore, sediment samples at a certain location were taken around low tide, and samples at a similar and close by location were sampled two hour after low tide. This might reduce the discrepancy between chl *a* amounts measured in the field and amounts appearing on the imagery. Furthermore, the issue of moisture content needs to be taken into account, as with the difference between the image acquisition time and the field sampling, the moisture content might change. This will also be considered in the future campaigns of ALGASED where the sampling would occur at different stages in reference to low tide (at low tide and two hours after low tide).

The BPC code was able to classify most of the images, yet the amount of field data used for training needs to be increased. This can be done by obtaining more field data in upcoming campaigns and by reducing the number of classes to be characterized per property. In any case, the spectra of the resulting classes were quite similar to the reference spectra for most properties and most imagery.

Throughout this report, it was shown that using five selected bands from different parts of the spectrum can lead to similar or better results than using all the bands on the hyperspectral data. Furthermore, the feature selection of the BPC code shows that to characterize each sediment property, only a few bands are required. To characterize the four sediment properties simultaneously, the bands chosen lied all over the visible, NIR, and SWIR parts of the spectrum. Therefore, only a few bands from different parts of the spectrum can be sufficient for an acceptable classification.

6 References

Adam, S., and Vitse, I., Johannsen, C., and Monbaliu, J., 2006, Sediment type unsupervised classification of the Molenplaat, Westerschelde estuary, the Netherlands. EARSeL eProceedings, 5:146 - 160

Deronde, B., Kempeneers, P. and Forster, R., 2006, Imaging spectroscopy as a tool to study sediment characteristics on a tidal sandbank in the Westerschelde. Estuarine, Coastal and Shelf Science, 69, 580-590

Ibrahim, E. and Monbaliu, J., 2008, Assessment of Unsupervised Classification Techniques for Intertidal Sediments, An internal report of ALGASED

Ibrahim, E. and Monbaliu, J., 2009a, A Description of the Hyperspectral Imagery of ALGASED, pp. 21, contribution to WP6 (internal report) of ALGASED

Ibrahim, E. and Monbaliu, J., 2009b, Unsupervised classification vs. supervised classification of hyperspectral images of ALGASED, pp. 18, contribution to WP5 of ALGASED

Ibrahim, E., Adam, S., De Wever, A., Dasseville, R., Forster, R., Sabbe, K., Wal, van der D., Monbaliu, J., 2009, Field campaigns and field data report, contribution to WP6 (internal report) of ALGASED

Kumar, S., Ghosh, J. and Crawford, M., 2000, A Bayesian Pairwise Classifier for Character Recognition, in Cognitive and Neural Models for Word Recognition and Document Processing, Nabeel Mursheed (Ed), World Scientific Press

Kruse, F. A., Lefkoff, A. B., Boardman, J. B., Heidebrecht, K. B., Shapiro, A. T., Barloon, P.J., and Goetz, A. F. H., 1993, The Spectral Image Processing System (SIPS) - Interactive Visualization and Analysis of Imaging spectrometer Data, Remote Sensing of the Environment, 44, 145 - 163

Lillesand, T.M. and Kiefer, R.W., 2000, Remote sensing and image interpretation, John Wiley & Sons